The 2014-15 eruption and the short-term geochemical evolution of the Fogo volcano (Cape Verde): Evidence for small-scale mantle heterogeneity

Article *in* Lithos · September 2017

DOI: 10.1016/j.lithos.2017.07.001

12 authors, including:

João Mata
University of Lisbon
171 PUBLICATIONS **975** CITATIONS

SEE PROFILE

Sofia Martins
IDL - Insituto D. Luís
35 PUBLICATIONS **170** CITATIONS

SEE PROFILE

Nadine Mattielli
Université Libre de Bruxelles
159 PUBLICATIONS **2,429** CITATIONS

SEE PROFILE

José Madeira
University of Lisbon
238 PUBLICATIONS **1,874** CITATIONS

SEE PROFILE

Lithos 288–289 (2017) 91–107

Contents lists available at ScienceDirect

Lithos

journal homepage: www.elsevier.com/locate/lithos

The 2014–15 eruption and the short-term geochemical evolution of the Fogo volcano (Cape Verde): Evidence for small-scale mantle heterogeneity

J. Mata [a,*], S. Martins [a], N. Mattielli [b], J. Madeira [a], B. Faria [c], R.S. Ramalho [a,d,e], P. Silva [a,f], M. Moreira [g], R. Caldeira [h], M. Moreira [a,f], J. Rodrigues [i], L. Martins [a]

[a] Instituto Dom Luiz, Faculdade de Ciências, Universidade de Lisboa, 1749-016 Lisboa, Portugal
[b] Laboratoire G-Time, DGES, Université Libre de Bruxelles, ULB, Av. Roosevelt, 50, CP, 160/02, 1050 Brussels, Belgium
[c] Instituto Nacional de Meteorologia e Geofísica, Mindelo, Cape Verde
[d] School of Earth Sciences, University of Bristol, Wills Memorial Building, Queen's Road, Bristol BS8 1RJ, UK
[e] Lamont-Doherty Earth Observatory at Columbia University, Comer Geochemistry Building, 61 Route 9W, P.O. Box 1000, Palisades, NY 10964-8000, USA
[f] Instituto Politécnico de Lisboa, ISEL/ADF, Lisboa, Portugal
[g] Institute de Physique du Globe de Paris, France
[h] Laboratório Nacional de Energia e Geologia, I.P., 2610-999 Amadora, Portugal
[i] Cape Verde

ARTICLE INFO

Article history:
Received 30 July 2016
Accepted 1 July 2017
Available online 13 July 2017

Keywords:
2014–15 Fogo Island (Cape Verde) eruption
Ocean island basalts
Mantle heterogeneity
Short-term magmatic variation
Volcano plumbing system

ABSTRACT

Recurrent eruptions at very active ocean island volcanoes provide the ideal means to gain insight on the scale of spatial variations at the mantle source and on temporal changes of magma genesis and evolution processes. In 2014, after 19 years of quiescence, Fogo volcano (Cape Verde Archipelago) experienced a new eruption, with the vents located 200 m from those of the 1995 eruption, and less than 2000 m from those of the 1951 event. This offered a unique opportunity to investigate the existence of small-scale mantle heterogeneities and the short-term compositional evolution of magmas erupted by a very active oceanic volcano like Fogo. Here we present petrological and geochemical data from the early stages of the Fogo's most recent eruption – started on November 23, 2014 – and compare them with the signature of previous eruptions (particularly those of 1995 and 1951).

The magmas erupted in 2014 are alkaline (up to 23.4% and 0.94% of normative *ne* and *lc*, respectively) with somewhat evolved compositions (Mg # < 56), ranging from tephrites to phonotephrites. The eruption of phonotephritic lavas preceded the effusion of tephritic ones. Lavas carried to the surface clinopyroxene and kaersutite phenocrysts and cognate megacrysts, which indicate that the main stages of magma evolution occurred in magma chambers most probably located at mantle depths (25.6 ± 5.5 km below sea level). This was followed by a shallower (<1.5 km below sea level) and shorter (≈50 days) magma stagnation before the eruption. 2014 magmas have more unradiogenic Sr and more radiogenic Nd compositions than those of the previous 1951 and 1995 eruptions, which generally have less radiogenic Pb ratios. These isotopic differences – coming from quasi-coeval materials erupted almost in the same place – are remarkable and reflect the small-scale heterogeneity of the underlying mantle source. Moreover, they reflect the limited isotopic averaging of the source composition during partial melting events as well as the inefficient homogenization within the plumbing system when on route to the surface. The lid effect of an old and thick lithosphere is considered of utmost importance to the preservation of a significant part of source heterogeneity by erupted magmas. The decrease in the contribution of an enriched component to the Fogo magmas in the 2014 eruption marks a change on the volcano short-term evolution that was characterized by a progressive increase of the importance of such a component. Nb/U ratios of the 2014 lavas are similar, within 2σ, to the mean value of OIB, but significantly lower than those reported for the 1995 and 1951 eruptions. This is considered to reflect the lack of significant mixing of the 2014 magmas with lithospheric melts, as opposed to what is here hypothesised for the two previous eruptions.

1. Introduction

The Earth's mantle is highly heterogeneous as depicted by the composition of oceanic basalts and particularly by those from oceanic

* Corresponding author.
E-mail address: jmata@fc.ul.p (J. Mata).

http://dx.doi.org/10.1016/j.lithos.2017.07.001
0024-4937/

islands (e.g. Hofmann, 2003; White, 2015). Such heterogeneity is considered the result of mixing in different proportions of the so-called mantle components (e.g. Stracke et al., 2005; Zindler and Hart, 1986). The length scale of mantle heterogeneities sampled by oceanic basalts is highly variable, sometimes encompassing large regional domains (e.g. DUPAL and SOPITA anomalies; Hart, 1984; Staudigel et al., 1991; White, 2015), but being also evident at the scale of a single magmatic province, as reported, for example, for the Azores (e.g. Beier et al., 2008), Cape Verde (Doucelance et al., 2003; Gerlach et al., 1988) and Galápagos (Gibson et al., 2012) archipelagos. The same is true at the scale of a single island edifice (e.g. Barker et al., 2010; Mourão et al., 2012a; Nobre Silva et al., 2013), even when considering quasi-coeval magmatic products (e.g. Madureira et al., 2011).

In this work we evaluate the small-scale heterogeneity of the mantle source feeding a plume-related intraplate volcano, as well as the short-term geochemical evolution of the magmas it generated. To this purpose we use as a case study the island of Fogo (Cape Verde Archipelago), one of the most active oceanic volcanoes in our planet. Indeed, since the mid-15th Century, Fogo experienced about 27 eruptions mostly from vents located within a restricted area (≈50 km^2) of the island's summit depression (Fig. 1). The latest eruption occurred in 2014–2015 and constitutes the main object of this study. Their vents are practically coincident or localized less than 2 km away from those of the two previous eruptions (1995 and 1951, respectively). For this reason, Fogo constitutes a prime locality to test the existence of small-scale heterogeneities of mantle sources, as well as to investigate the recent short-term evolution of magmas issued from those sources. Here we characterize and discuss the geochemistry of the lava flows and pyroclasts extruded during the initial stages of the eruption (up to December 7, 2014). Even though we are only considering lavas formed during the first 15 out of 60 days of eruption, the extracted information allows the demonstration of significant chemical differences relative to the products erupted in 1951 and 1995. The preservation of such heterogeneities by magmas is also here discussed emphasizing the role of lithosphere thickness.

The mineralogical, geochemical and physical characteristics of a volcano are partially constrained by what happens during magma transit from its source to the surface, i.e. by the nature and dynamics of the associated magma plumbing system (e.g. Cashman et al., 2017; Cooper, 2017; Klügel et al., 2015; Longpré et al., 2008). The Fogo's plumbing system is here assessed using barometric data, which indicates a location of the main magma chamber(s) into the mantle.

Our observations show that magmas erupted in 2014 mark a reversal from the tendency depicted by previous eruptions (Escrig et al., 2005), which exhibited an increasing contribution of a local end-member with relatively radiogenic Sr.

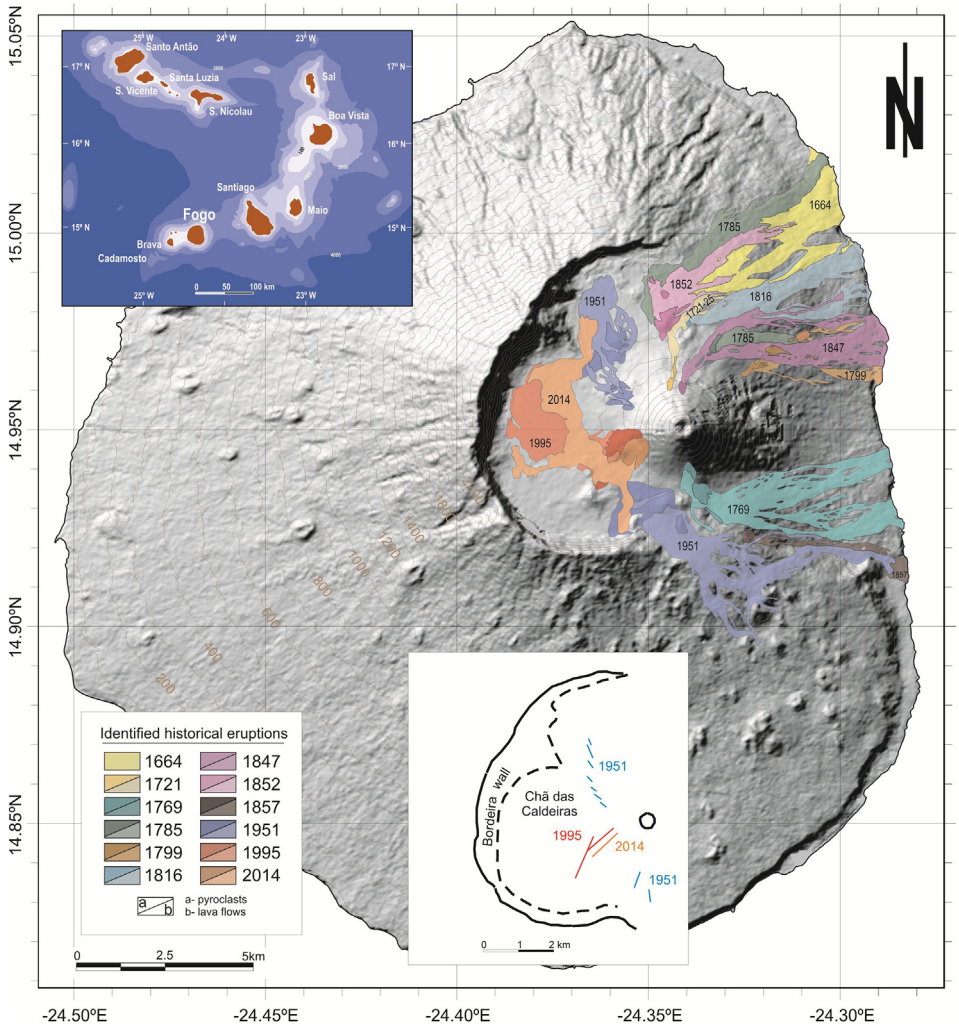

Fig. 1. Geological map of the identified historical eruptions in Fogo (modified from Torres et al., 1998) superimposed on the digital terrain model of the island. The upper inset shows the location of the Island of Fogo in the archipelago of Cape Verde. The lower insets correspond to the legend of the geological map and to a structural sketch showing the geometry and location of the eruptive fissures of the last three eruptions (1951, 1995 and 2014/15), the Bordeira wall (continuous line represents the top; dashed line represents the base), and the crater rim of Pico do Fogo.

2. Cape Verde geological setting

The Cape Verde Archipelago (Eastern Central Atlantic; Fig. 1) lies on top of the largest intraplate bathymetric anomaly in the Earth's oceans – the Cape Verde Rise – that coincides with important geoid, heat flow, gravity, and seismic anomalies (e.g. Courtney and White, 1986; Dash et al., 1976; Liu and Zhao, 2014; Wilson et al., 2013). The archipelago, which stands on 120–140 Ma-old seafloor (Williams et al., 1990) is regarded as a hotspot resulting from the impingement of a mantle plume on the quasi-stationary (<1 cm·a^{-1} in the region; Holm et al., 2008; Pollitz, 1991) Nubian plate. This would explain the long-lasting volcanic activity and, at least partially, the age distribution of volcanism and the geometry of both the archipelago and the Cape Verde Rise (Holm et al., 2008; Lodge and Helffrich, 2006; Madeira et al., 2008; Ramalho, 2011; Ramalho et al., 2010). The presence of a mantle plume deeply anchored in the lower mantle is suggested by seismic data (Forte et al., 2010; French and Romanowicz, 2015; Montelli et al., 2006; Saki et al., 2015; Vinnik et al., 2012) and of noble gas studies performed on carbonatites and alkaline silicate rocks (Christensen et al., 2001; Doucelance et al., 2003; Mata et al., 2010; Mourão et al., 2012b). The oldest exposed hotspot-related volcanism is ~26 Ma (Torres et al., 2010) and at least three islands are considered volcanically active (Santo Antão, Brava and Fogo; see e.g. Eisele et al., 2015; Faria and Fonseca, 2014; Madeira et al., 2010) but only Fogo had post-settlement eruptions.

Magmatism in Cape Verde is strongly alkaline, as testified by the occurrence of nephelinitic, melanephelinitic, and melilititic rocks on several islands. It is also well known by its striking geochemical heterogeneity, allowing the isotopic separation of the islands into two groups (Northern and Southern). Lavas from the Southern group have more radiogenic Sr, but unradiogenic Nd and Pb ratios than those from the Northern group, which exhibit more unradiogenic He signatures. In addition, magmatic rocks from the Southern group are positioned, on the $^{208}Pb/^{204}Pb$ vs. $^{206}Pb/^{204}Pb$ diagram, above the Northern Hemisphere Reference Line (NHRL; Hart, 1984) whilst lavas from the Northern group tend to plot along the NHRL (e.g. Doucelance et al., 2003; Gerlach et al., 1988; Holm et al., 2006; Kogarko and Asavin, 2007; Martins et al., 2010; Mourão et al., 2012a and references therein). Notable exceptions to this scenario include Brava (the southwesternmost island), which depicts both typical Northern (older sequences) and Southern (younger volcanism) isotope signatures (Mourão et al., 2012a), and the neighbouring Cadamosto seamount, which also presents typical Northern signatures (Barker et al., 2012).

2.1. Fogo volcano

Fogo is one of the youngest of the Cape Verde Islands and a very prominent oceanic volcano, standing ~7 km above the surrounding seafloor. The island exhibits a slightly asymmetric conical shape, being truncated atop by a summit depression open to the east. This 8 km-wide depression - Chã das Caldeiras - is surrounded on three sides by an almost vertical wall – the Bordeira – up to 1 km tall. Inside the summit depression and on its eastern side, a 1100 m high strato-volcano – Pico do Fogo – grew up to an elevation of 2829 m (Fig. 1). Fogo volcano is therefore interpreted as a compound volcano, featuring a "somma-vesuvio" association of a younger strato-cone on top of an older, collapsed volcanic edifice (Foeken et al., 2009; Ribeiro, 1954). The opening to the east of the summit depression is interpreted as the result of a massive flank collapse (Brum da Silveira et al., 2006; Day et al., 1999), as attested by a landslide debris deposit extending offshore into the channel between Fogo and Santiago (e.g. Masson et al., 2008), and by field evidence documenting the impact of a megatsunami in the neighbouring island of Santiago (Paris et al., 2011; Ramalho et al., 2015). The present-day Pico do Fogo stands on, and partially fills, the collapse scar, and naturally post-dates the collapse event, which is interpreted to have occurred either at ~117 or at ~73 ka (cf. Eisele et al., 2015; Ramalho et al., 2015). An older basement is, however, exposed in two shallow valleys near the city of São Filipe, where plutonic calciocarbonatites were dated from 2.5 Ma to 5.1 Ma (Foeken et al., 2009; Hoernle et al., 2002; Madeira et al., 2005). These suggest a >2 Myr volcanic hiatus in the evolution of Fogo.

Fogo volcano is very active, with 27 eruptive events since 1500 AD (Ribeiro, 1954). The mean recurrence interval between eruptions is 19.8 years, but with individual intervals ranging from 1 to 94 years. Historical eruptions seem to have been confined to Chã das Caldeiras and the eastern slope of the volcano, as it was the case of the recent 1951, 1995 and 2014/2015 events (Fig. 1).

The latest eruption started on November 23, 2014 and continued until February 7, 2015. The eruption occurred on a NE–SW trending 700 m-long fissure located on the SE flank of the previous 1995 cinder cone, an adventitious vent developed on the SW flank of Pico do Fogo (Fig. 2A, B and D). This eruption started with vigorous "hawaiian" fire-fountain activity, followed by strombolian activity, and later by simultaneous or alternating hawaiian (Fig. 2C), strombolian and vulcanian (Fig. 2D) eruptive activity from different craters along a fissural vent, lasting for several days. The eruption also emitted, from the first day, thick a'a lava flows (Fig. 2E; Supplementary Material S1) forming two initial lava lobes. A shorter lobe, 1.7 km-long, progressed southwestwards down to the flank of Cova Tina cone, stalling short of the Bordeira wall in this area. The second, longer lobe advanced 3 km to the northeast in the initial hours of the eruption, crossing the topographic barrier formed by the 1995 lava flows by advancing through the existing road cut. It advanced intermittently towards the village of Portela, causing widespread destruction (Fig. 2F). During the later stages of the eruption, thinner, more fluid, a'a and especially pahoehoe breakouts expanded the flow field to the west and north, the latter descending to the village of Bangaeira, destroying almost completely both villages and reaching a total length of 5.2 km (Fig. 1). Overall, the resulting lava flows, with an average thickness of about 9 m, covered an area of 4.8 km^2, with extruded volumes estimated to correspond to ~45×10^6 m^3, at a mean eruption rate of 6.8 m^3.s^{-1} (Bagnardi et al., 2016; Richter et al., 2016). Lava flow thicknesses as high as 35 m (close to the vent), or 25 m on the lava ponding west of Portela, were described by Richter et al. (2016). See also Cappello et al. (2016) for additional information about the eruption.

3. Analytical procedures

Whole-rock major and trace element concentrations were obtained at Activation Laboratories, Ltd. (Ancaster, Ontario, Canada) using the geochemical analytical package 4Lithoresearch (lithium metaborate/tetraborate fusion - ICP and ICP/MS).

Several certified reference materials from USGS (United States Geological Survey), GSJ (Geological Survey of Japan) and CCRMP (Canadian Certificate Reference Material Project) were run to check for accuracy (Supplementary Material S2). Errors associated with the accuracy are ≤4% for major elements and better than 9% for the REE and the most widely used incompatible elements. Reproducibility was generally better than 5% for both major and trace elements. For detailed information regarding analytical and control procedures consult the Actlabs website (www.actlabs.com).

Mineral analyses were performed on carbon-coated polished thin sections using a JEOL SUPERPROBE™, model JXA-8200, in wavelength dispersive mode at the Departamento de Geologia da Faculdade de Ciências da Universidade de Lisboa (Portugal). Minerals were analysed with an acceleration voltage of 15 kV and a current of 25 nA, using a 5 μm wide beam for most minerals. Plagioclase and apatite were analysed using a 7 and 9 μm wide beam, respectively. The analyses performed in each mineral phase/glass were calibrated using the composition of reference material, with precisions being better than 2% and ordinarily around 1% (see Supplementary Material S3-H for specific minerals standards used in each mineral analysis).

Fig. 2. Photos of the 2014/15 Fogo eruption: A- general view looking East of Pico do Fogo with the active vents at the base of the cone, the flat region of Chã das Caldeiras covered with the 1995 and 2014 lava flows and the south-eastern tip of the Bordeira wall; the eruptive column rises 3 km above the vents and is dispersed by south-eastward wind at an altitude of approximately 5 km (photo taken on November 29, 2014, at 15:44 UTC); B- the alignment of active vents, viewed from the south, during a low activity phase; the new cone is growing against the southeast flank of the 1995 cone (to the left); the lava flow is being fed by the southernmost vent; the lava flow at the base of the cone presents a lava channel and several skylights with degassing white columns (photo taken on December 2, 2014, at 19:35 UTC); C- night aspect of the central crater projecting plastic spatter fragments from the explosion of lava bubbles during an hawaiian lava lake phase (photo taken on November 28, 2014, at 20:48 UTC); D- aspect of vulcanian activity at the northernmost vent producing ash-laden episodic eruptive columns with the wind blowing from the north; the white plume marks the position of the effusive south vent (photo taken on November 30, 2014, at 19:24 UTC); E- aspect of the surface of the active lava flow seen from the northwest presenting strong thermal emission and degassing (photo taken on November 29, 2014, at 15:48 UTC); F- the village of Portela invaded by the front of the lava flow 3.5 km away from the effusive vent (photo taken on December 2, 2014, at 14:39 UTC). For more photos see Supplementary Material S1.

Isotopic analyses of Pb, Nd, Sr and Hf were performed at the Laboratoire G-Time of the Université Libre de Bruxelles (ULB, Belgium) on a Nu Plasma I Multi-Collector Inductively Coupled Plasma Mass Spectrometer (MC-ICP-MS) (@ Nu instruments).

Sr analyses were performed in wet mode. In routine, the raw data was normalized to $^{86}Sr/^{88}Sr = 0.1194$, and corrected for mass bias by standard sample bracketing using the lab's in-house Sr standard solution. The in-house shelf Sr standard was calibrated and normalized to the certified value of NBS 987 Sr standard (0.710248) reported by Weis et al. (2006). During our analytical sessions, in-house standard solution was run every two samples and gave an average value of 0.710287 ± 50 (2σ) for raw $^{87}Sr/^{86}Sr$ data (21 runs).

Nd and Hf were run in dry mode with an Aridus II desolvating system. To monitor the instrumental mass bias during the analysis sessions, the standard sample bracketing method was also applied. Standards were systematically run between every two samples, giving an average value in $^{143}Nd/^{144}Nd$ of 0.511921 ± 41 (2σ, 8 runs) for the Rennes Nd standard, and $^{176}Hf/^{177}Hf = 0.282172 \pm 30$ (2σ, 10 runs) for the JMC 475 Hf standard. The Nd and Hf isotopic measurements were internally normalized to $^{146}Nd/^{144}Nd = 0.7219$ and $^{179}Hf/^{177}Hf = 0.7325$, respectively. All Hf and Nd isotopic data (Table 1) are normalized to the reference values of 0.511961 and 0.282160 as published by Chauvel and Blichert-Toft (2001) and Chauvel et al. (2011).

For the Pb isotope analyses, a Tl dopant solution was added for every sample and standard, within a Pb-Tl concentration ratio of $\pm 5{:}1$ (for a minimum signal of 100 mV in the axial collector - ^{204}Pb). ^{202}Hg is routinely monitored to correct for the potential isobaric interference of ^{204}Hg on ^{204}Pb. Mass discrimination was monitored using ln – ln plots and corrected by the external normalization and the standard sample bracketing technique using the recommended values of Galer and Abouchami (1998) (i.e. $^{206}Pb/^{204}Pb = 16.9405 \pm 15$; $^{207}Pb/^{204}Pb = 15.4963 \pm 16$; $^{208}Pb/^{204}Pb = 36.7219 \pm 44$). The repeated measurements of the NBS981 gave the following values: $^{206}Pb/^{204}Pb = 16.9403 \pm 8$, $^{207}Pb/^{204}Pb = 15.4961 \pm 10$, $^{208}Pb/^{204}Pb = 36.7217 \pm 31$ (2σ) for the NBS981 Pb standard (5 runs).

4. Results

The samples used in this study were collected during a field survey undertaken during the course of the last Fogo eruption, between November 27 and December 7, 2014. From all collected samples a sub-

Table 1
Whole rock chemical analyses of 2014 erupted lava flows and pyroclasts.

Sample	F14–1	F14–2	F14–4	F14–5	F14–6	F14–7	F14–8	F14–9	F14–10	F14–11	F14–12	F14–13	F14–14
	Lava	Lava	Lava	Lava	Lava	Lava	Lava	Lava	Lava	Pyroc.	Pyroc.	Pyroc.	Pyroc.
Lithotype	Pht	Pht	Tep	Tep	Tep	Tep	Tep	Tep	Tep	Tep	Tep	Tep	Tep
SiO_2 (wt%)	47.99	47.74	45.19	43.54	43.03	44.70	45.10	45.07	44.03	44.62	44.16	43.10	44.40
TiO_2	2.50	2.54	3.16	3.58	3.81	3.37	3.31	3.17	3.46	3.34	3.38	3.71	3.37
Al_2O_3	19.28	18.53	17.58	16.80	15.35	16.86	16.85	17.58	16.54	16.84	16.80	16.28	16.66
Fe_2O_3*	2.12	2.26	2.28	2.53	2.74	2.40	2.36	2.32	2.54	2.47	2.51	2.66	2.47
FeO*	6.06	6.46	7.61	8.44	9.12	7.99	7.86	7.73	8.48	8.24	8.36	8.88	8.22
MnO	0.21	0.22	0.21	0.22	0.21	0.22	0.22	0.22	0.22	0.22	0.22	0.21	0.22
MgO	2.93	3.08	4.47	5.25	6.33	4.91	4.63	4.43	5.15	4.55	4.83	5.66	4.87
CaO	7.96	8.21	9.95	10.95	11.98	10.47	10.30	9.83	10.82	10.51	10.62	11.43	10.74
Na_2O	6.00	6.00	5.06	4.51	3.84	4.78	4.95	5.13	4.55	4.76	4.69	4.01	4.64
K_2O	4.17	4.16	3.48	3.09	2.64	3.29	3.39	3.51	3.12	3.31	3.30	2.97	3.26
P_2O_5	0.78	0.80	1.00	1.11	0.96	1.02	1.05	1.02	1.10	1.14	1.14	1.10	1.15
LOI	−0.17	−0.18	−0.26	−0.42	−0.53	−0.4	−0.37	−0.30	−0.51	−0.09	0.65	−0.04	−0.19
Mg#	46.25	45.98	51.14	52.58	55.32	52.26	51.21	50.53	51.97	49.63	50.75	53.16	51.34
S (%)	0.012	0.008	0.007	0.006	0.009	0.009	0.008	0.009	0.008	0.023	0.012	0.023	0.022
Sc (ppm)	5	5	11	15	23	13	12	11	14	11	12	17	13
V	217	223	280	322	363	306	299	286	322	300	305	353	311
Cr	30	<20	40	60	90	50	50	60	50	70	30	30	20
Co	17	20	26	30	37	28	27	26	29	28	29	34	29
Ni	6	20	17	22	42	21	19	17	31	15	16	28	17
Rb	97	108	79	68	58	76	78	79	70	75	75	65	72
Sr	1408	1403	1256	1213	1084	1242	1280	1295	1212	1243	1194	1140	1214
Y	27.40	31.70	29.40	29.40	27.60	29.80	29.80	29.10	29.90	30.20	30.20	28.90	29.90
Zr	433	422	394	382	336	394	406	412	384	387	374	360	390
Nb	117	133	112	98.4	89	110	112	111	107	113	108	97.4	110
Cs	1.10	1.20	0.90	0.80	0.60	0.80	0.90	0.90	0.80	0.80	0.80	0.70	0.80
Ba	1198	1204	1043	973	839	1013	1050	1076	1000	1025	1013	960	1024
La	81.30	103.00	78.00	71.10	61.30	75.10	77.00	78.10	73.10	78.40	77.30	67.80	76.10
Ce	157	199	157	147	129	155	156	158	152	160	159	141	155
Pr	17.80	22.20	18.50	17.70	15.70	18.50	18.40	18.80	18.10	18.90	19.10	17.10	18.70
Nd	64.20	78.90	68.90	68.30	61.40	69.30	70.60	70.90	69.20	72.60	72.50	66.20	71.80
Sm	10.60	12.70	11.80	12.00	11.20	12.00	12.40	12.20	12.30	12.50	12.50	11.80	12.40
Eu	3.39	4.03	3.90	3.96	3.62	3.93	4.08	3.92	3.93	4.02	4.11	3.83	3.99
Gd	7.59	9.02	9.41	9.30	8.61	9.03	8.95	9.11	9.19	9.10	9.27	9.21	9.31
Tb	1.07	1.24	1.23	1.24	1.16	1.22	1.26	1.22	1.26	1.29	1.29	1.24	1.28
Dy	5.91	6.82	6.60	6.63	6.35	6.61	6.69	6.56	6.61	6.79	6.78	6.30	6.61
Ho	1.05	1.22	1.19	1.20	1.11	1.14	1.19	1.17	1.21	1.19	1.23	1.16	1.19
Er	2.90	3.25	3.08	3.11	2.86	3.06	3.04	3.07	3.01	3.05	3.10	2.99	3.09
Tm	0.38	0.43	0.39	0.41	0.35	0.41	0.40	0.41	0.40	0.41	0.42	0.38	0.40
Yb	2.30	2.64	2.33	2.16	2.03	2.35	2.39	2.30	2.23	2.27	2.34	2.13	2.28
Lu	0.33	0.37	0.33	0.32	0.29	0.32	0.33	0.31	0.31	0.31	0.34	0.29	0.31
Hf	6.50	7.40	6.90	6.90	6.80	7.00	7.00	7.30	7.30	7.00	6.40	6.80	7.10
Ta	7.85	8.70	7.65	7.04	6.13	7.49	7.61	7.75	7.32	7.63	7.59	6.70	7.50
Th	9.38	11.20	8.09	6.83	5.62	7.58	7.59	7.95	7.15	7.54	7.54	6.24	7.32
U	2.41	2.64	1.98	1.64	1.40	1.84	1.87	1.92	1.74	1.95	1.91	1.49	1.81

* Fe_2O_3/FeO ratio calculated from the analysed $Fe_2O_3^T$ by the method of Middlemost (1989).

set of 14 was selected for petrographic, mineralogical and whole-rock elemental geochemical study (Table 1), on the basis of its geographical and temporal distribution. Sr, Nd, Hf and Pb isotopes were determined for 8 samples (Table 2), while the He isotope analysis was performed for one sample. On the Supplementary Material the reader can also find mineral chemistry data (S3) and the whole-rock normative compositions (S4). The composition of interstitial glasses determined by electron microprobe is also presented on Supplementary Material S3-G.

4.1. Petrography and mineral chemistry

On a chemical basis, lava flows and pyroclasts erupted up to December 7 are, sensu lato, tephrites and phonotephrites (see Section 4.3 and Fig. 3). Some of the most important petrographic characteristics of the studied samples are depicted on Fig. 4 and their mineral chemistry data are displayed on the Supplementary Material S3.

Table 2
Isotope analyses for selected samples.

	$^{87}Sr/^{86}Sr$	$^{143}Nd/^{144}Nd$	$^{176}Hf/^{177}Hf$	$^{206}Pb/^{204}Pb$	$^{207}Pb/^{204}Pb$	$^{208}Pb/^{204}Pb$	ε_{Nd}	ε_{Hf}	Δ7/4	Δ8/4
F14–1	0.703655 ± 15	0.512774 ± 7	0.282940 ± 5	18.9901 ± 08	15.5642 ± 7	38.8462 ± 19	2.65	5.93	1.47	26.01
F14–2	0.703669 ± 12	0.512769 ± 7	0.282946 ± 5	18.9993 ± 09	15.5625 ± 8	38.8509 ± 23	2.55	6.15	1.20	25.38
F14–5	0.703689 ± 10	0.512762 ± 8	0.282954 ± 4	18.9811 ± 10	15.5588 ± 9	38.8470 ± 24	2.43	6.42	1.03	27.19
F14–6	0.703638 ± 09	0.512781 ± 7	0.282951 ± 5	18.9766 ± 10	15.5618 ± 9	38.8578 ± 21	2.79	6.33	1.37	28.80
F14–7	0.703613 ± 09	0.512789 ± 8	0.282946 ± 5	18.9717 ± 10	15.5632 ± 9	38.8341 ± 23	2.94	6.15	1.57	27.03
F14–10	0.703647 ± 10	0.512772 ± 7	0.282959 ± 5	18.9799 ± 07	15.5611 ± 7	38.8467 ± 15	2.62	6.62	1.27	27.30
F14–11	0.703656 ± 10	0.512773 ± 7	0.282938 ± 4	19.0008 ± 10	15.5609 ± 8	38.8553 ± 22	2.63	5.88	1.03	25.63
F14–14	0.703626 ± 09	0.512769 ± 6	0.282958 ± 5	18.9859 ± 09	15.5590 ± 7	38.8480 ± 18	2.55	6.57	0.99	26.70

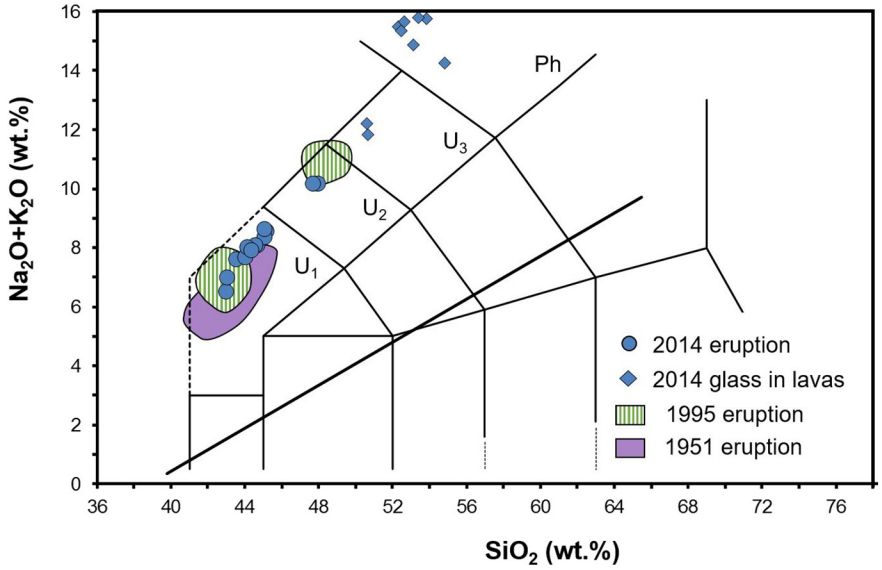

Fig. 3. Total alkali-silica (TAS) diagram (Le Maitre, 2002) for the 2014 magmatic rocks and interstitial glass occurring in the matrix of the lava samples. The thick line is a compositional divider between alkaline and subalkaline volcanic rocks (MacDonald, 1968). The compositional fields of the 1951 and 1995 are also shown for comparison (data from Doucelance et al., 2003; Escrig et al., 2005; Hildner et al., 2011;). U1, U2, U3 and Ph correspond to the field designations of Le Maitre et al. (2002) (U1: Tephrite/Basanite; U2: Pnotephrite; U3: Tephriphonolite; Ph: Phonolite). See the main text (Section 4.3) for details on the systematics.

4.1.1. Tephrites

The bulk (≈ 85%) of the eruptive products corresponds to tephrites. The lavas are vesicular and porphyritic with a hypocrystalline groundmass and with phenocrysts amounting up to 10% of the rock volume. Samples are highly vesicular (up to 60% of the rock volume) and the vesicles are irregular in shape and size.

The most abundant phenocryst phase is clinopyroxene. Even though all the clinopyroxene phenocrysts are classified as diopside ($Wo_{49}En_{38}Fs_{13}$ to $Wo_{52}En_{36}Fs_{12}$) according to IMA recommendations (Supplementary Material S-3A), in most samples two groups must be considered regarding size and composition. One group corresponds to phenocrysts with dimensions up to 2 mm and euhedral shapes. They are characterized by normal zoning patterns, with Al_2O_3, FeO and TiO_2 increasing and MgO and Mg# decreasing from core to rim. Opaque mineral inclusions are frequent. The other group of phenocrysts occurs in clusters along with kaersutite, both with dimensions up to 4 mm in length. Clinopyroxene megacrysts in these aggregates usually show complex zoning patterns presenting abnormal compositional variations with increments of Al_2O_3, FeO and TiO_2 towards the intermediate zone/mantle and then decreasing towards the rim; the opposite occurs with MgO, suggesting a more complex and multistage crystallization history as compared with the first group. Indeed the increase in MgO/FeO and decrease in TiO_2 towards the rim is suggestive of a replenishment of the magma chamber where these particular crystals were formed, reflecting an influx of less evolved magmas, thus pointing out to mixing of distinct magma batches. However, both groups of clinopyroxenes show similar Al^{VI} values (0.059 to 0) and Al/Ti ratios indicating that megacrysts are cognate, being genetically related with the host lava and with the clinopyroxene phenocrysts. This assertion is also considered valid for keaersutite megacrysts given the chemical evidence for amphibole fractionation (see 5.1).

These kaersutite crystals are Mg- and Ti-rich (MgO = 12.8–13.0 wt.%; TiO_2 up to 6.07 wt.%), usually occurring in association with apatite and showing reaction rims where clinopyroxene and rhönite crystals are present, sometimes completely replacing the amphibole (Fig. 4D). Olivine crystals are restricted to inclusions in clinopyroxene phenocrysts and to the groundmass. In all lava samples the opaque minerals can be considered microphenocryts, being characterized by euhedral shapes and dimensions up to 1 mm. Most of the occurring oxides can be considered as titanomagnetites, with ulvöspinel component (X_{USP}) up to 57, and Cr# ranging from 1.6 to 5.3 (see Supplementary Material S3-E).

The groundmass is made up of small crystals immersed in a glassy matrix. These comprise plagioclase laths (labradorite, $An_{56–66}$) sometimes with a fluidal arrangement, clinopyroxene elongated crystals ($Wo_{49}En_{37}Fs_{14}$ to $Wo_{53}En_{32}Fs_{15}$), finely disseminated opaque minerals (titanomagnetites, $58 < X_{USP} < 67$), rare olivine (Fo ≈ 72%), and fluorapatite (1.7 to 2.8 wt.% of F). The electron-microprobe analyses of interstitial glass revealed it to be very rich in alkalis (11.8 to 15.8 wt%, $K_2O + Na_2O$) and poor in MgO (down to 0.66 wt%) having tephriphonolitic and phonolitic (SiO_2 up to 54.15 wt%) compositions (see Fig. 3).

4.1.2. Phonotephrites

These lavas are vesicular hemicrystalline/hypocrystalline and sparsely porphyritic (phenocrysts up to 3% vol.). The vesicles are elongated reaching up to 10 mm in length and corresponding to 50 to 80% of rock volume. The clinopyroxene phenocrysts are euhedral, up to 3 mm in size, frequently showing complex oscillatory zoning patterns and inclusions of opaque minerals. Despite the striking optical zoning patterns, all the clinopyroxene phenocrysts are classified as diopside with a short compositional range ($Wo_{49}En_{35}Fs_{10}$ to $Wo_{53}En_{40}Fs_{14}$), being very similar to that reported for the tephrites. Olivine (Fo = 80–84%) is scarce, being identified only as a core inclusion in a clinopyroxene phenocryst. Microphenocrysts (up to 1 mm) of equant opaque minerals are classified as titanomagnetites (X_{USP} = 44–46; Cr# = 1.15–5.4). Kaersutite pseudomorphs are frequent. They consist of aggregates of rhönite and elongated clinopyroxene crystals, displayed in inward radial arrangements totally or partially replacing the amphibole. However, in either case, a border of small opaque minerals encloses the altered/partially altered amphibole crystals. These kaersuites are similar (MgO = 11.9–12.7 wt.%: TiO_2 up to 6.04 wt.%) to those occurring as megacrysts/phenocrysts in tephritic rocks, and the occurrence of apatite within or in close proximity to the amphibole is frequent. The groundmass is composed of plagioclase microliths (labradorite, $An_{54–66}$), elongated clinopyroxene crystals (average $Wo_{53}En_{31}Fs_{16}$), opaque minerals ($38 < X_{USP} < 57$; Cr# = 0.67–1.49), scarce olivine and glass.

In one sample, a cluster of clinopyroxene, opaque crystals, and amphibole is interpreted as a possible co-magmatic cumulate nodule. This interpretation is based on the large dimension of the crystals, the

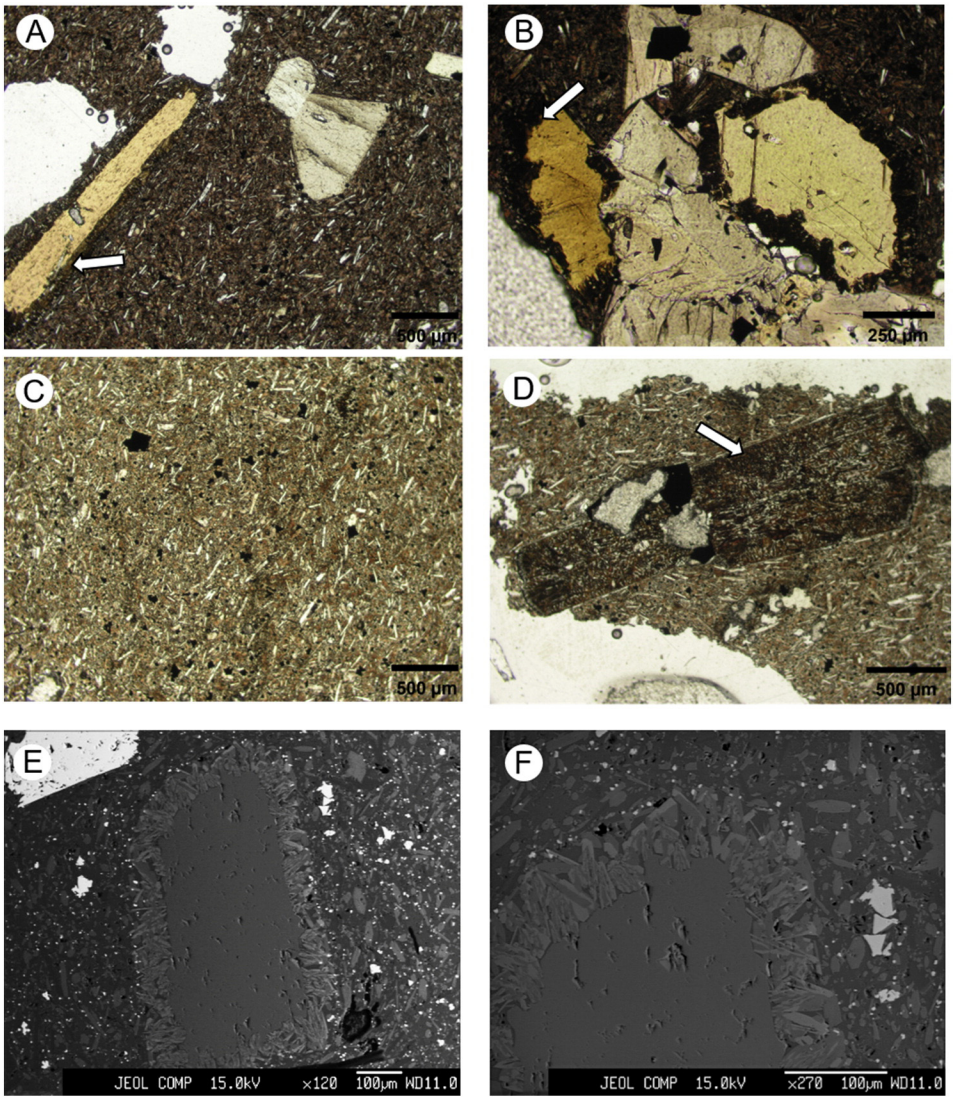

Fig. 4. Petrographic aspects of the lava flow samples showing the presence of clinopyroxene and kaersutite phenocrysts (A and B) in a hypocrystalline matrix with plagioclase, clinopyroxene and Fe-Ti oxides (A, B, C and D). Note the partial (A and B) or total (D) replacement of kaersutite by rhönite (opaque inosilicate of the aenigmatite group) which is marked by an arrow. Backscattered electron images showing a detailed view of the kaersutite rim replacement (E and F).

sharp contrast between the mineral aggregate and the surrounding rock matrix, and on the chemical similarity between its minerals and the rock phenocrysts. The same interpretation is considered for an aggregate of small (0.5 mm in length) plagioclase crystals characterized by anorthite content up to 79%. Ultramafic nodules of cumulate origin, mainly composed of olivine, clinopyroxene, and amphibole, were also reported for this eruption by Caldeira et al. (2015).

4.2. Whole rock elemental composition

Major and trace element analyses of the studied rocks are presented in Table 1, while normative compositions can be found in Supplementary Material S4.

As all other subaerial lavas in the Cape Verde Islands, Fogo's 2014 volcanic products are alkaline. They plot dominantly in the U_1 field, but also in the U_2 (phonotephrites) field of the TAS diagram (Fig. 3). Rocks plotting inside the U_1 field would be classified, according their CIPW normative composition, either as nephelinites (normative *ne* > 20%) – the dominant type – or as melanephelinites (normative *ne* < 20%; normative *ab* < 5%) according to the subdivision proposed by Le Bas (1989); (see S4). However, as modal plagioclase can be identified in most of the rocks plotting in the U1 TAS field and for all the samples normative *ol* < 10%, the classification as tephrites is here preferred and used.

The rocks are representative of moderately evolved magmas characterized by Mg# ranging from 55.32 to 45.98 and by Na_2O/K_2O between 1.35 and 1.46. The less evolved rocks (Mg# = 55.32 to 51.97) have TiO_2 contents varying from 3.65 to 3.75 wt%, P_2O_5 close to 1 (0.94 to 1.11 wt%), CaO/Al_2O_3 ratios ranging from 0.65 to 0.78 and K_2O/TiO_2 ratios between 0.25 and 0.32.

The 2014 lavas are highly enriched in the most incompatible elements (Fig. 5), which is depicted, for example, by $(La/Yb)_{cn}$ ratios >20, with the most evolved rocks presenting the highest values for this ratio (>23). Primitive mantle normalized incompatible elements patterns (Fig. 5c) show a significant enrichment of Nb and Ta relatively to the light REE and the radiogenic heat producers K, Th and U. Small Hf negative anomalies are also evident, which partially reflects the high Zr/Hf ratios (>49), well above the value of 36 characterizing CI chondrites and the primitive mantle (e.g. Palme and O'Neil, 2003).

The sampled pyroclasts and lava flows are similar in composition, the most significant difference being the sulphur-enriched composition of pyroclasts (120 to 230 ppm; $\overline{X}$ = 200 ppm) as compared to lava flows (60 to 120 ppm; $\overline{X}$ = 84 ppm). This indicates a more effective degassing of lava flows as a consequence of a slower cooling.

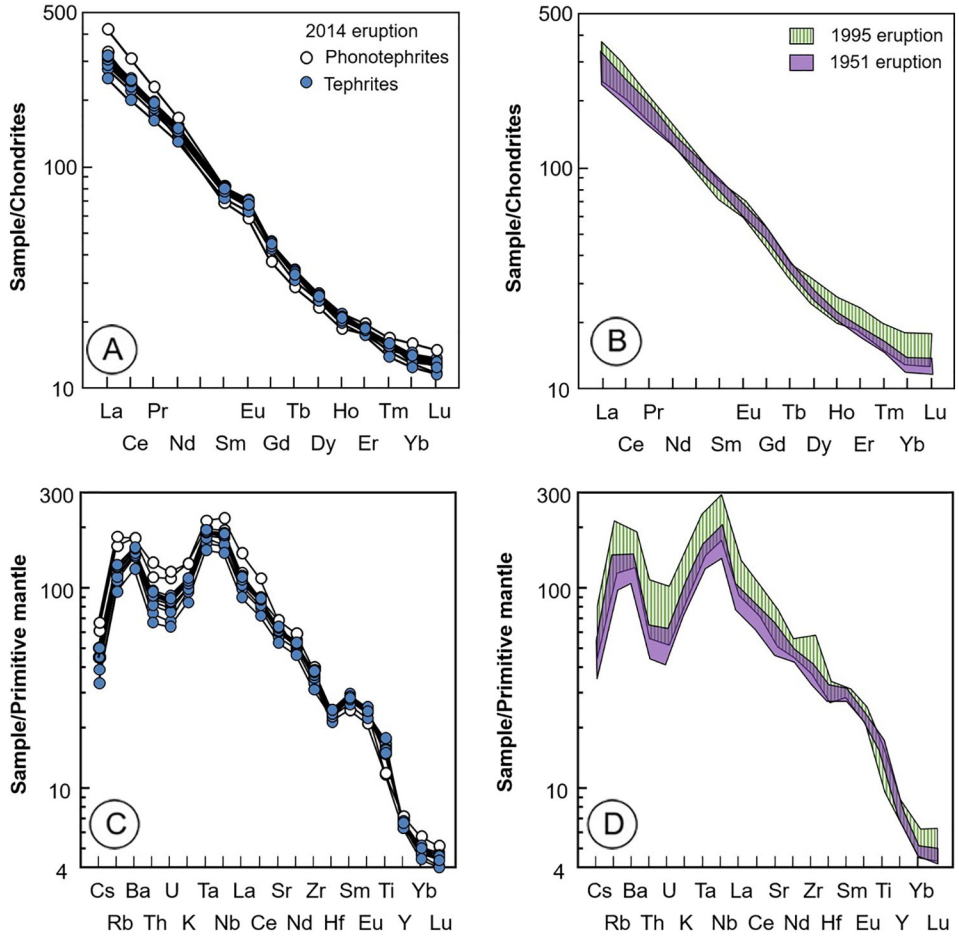

Fig. 5. Trace element characteristics of the 2014 eruptive products compared with those of the 1951 and 1995 eruptions (see Hildner et al., 2012 and Hildner et al., 2011, respectively). Normalizing values of Palme and O'Neil (2003).

Most of the characteristics described above are similar to those of lavas erupted during the two precedent eruptions (1995 and 1951), as Fig. 5 shows. Notwithstanding the fact that the samples here studied are only representative of the lava emitted during the first 15 days of the eruption, some differences, however, were noticed: i) the 1995 lavas present a slightly higher compositional range (MgO from 6.86 to 2.40 wt%; Hildner et al., 2011) than the ones from 2014 (MgO from 6.23 to 2.93 wt%); ii) from the three eruptions considered, the 1951 event produced the less evolved lavas (MgO up to 8.24 wt%; Hildner et al., 2012); iii) for the same SiO_2 content, the 1951 lavas tend to be less alkali-rich than the 2014 and 1995 volcanics (Fig. 3); iv) the 2014 and 1995 erupted materials are characterized by small compositional gaps ($\Delta SiO_2 = 2.5\%$ and 3.8%, respectively) in opposition to the described for from the 1951 eruption for which no phonotephrite compositions were reported (see Fig. 1 and references therein); v) for these three eruptions, the most evolved products are the phonotephrites from the 1995 eruption, which also present the highest concentrations in incompatible elements like Nb and Ta. However, the highest concentrations in light REE are found in phonotephrites from the 2014 eruption, which show the highest La/Nb ratios. This higher La/Nb are also observed for the less evolved rocks (MgO > 5 wt%), with 2014 lavas presenting $\overline{X}$ La/Nb = 0.69, whereas the 1995 and 1951 less evolved rocks show $\overline{X}$ La/Nb = 0.60 (cf. Table 1, Hildner et al., 2011, 2012).

4.3. Whole rock isotope composition

The results of Sr, Nd, Hf and Pb isotope analyses are shown on Table 2. The lavas erupted in 2014 at Fogo Island present isotope signatures akin to those typical of the Southern islands in the Cape Verde Archipelago. Indeed, in opposition to what is observed for the Northern capeverdean islands (Fig. 6), they are characterized by relatively unradiogenic $^{206}Pb/^{204}Pb$ ratios (up to 19.001) and plot above the Northern Hemisphere Reference Line (Δ7/4 from 0.99 to 1.57; Δ8/4 from 25.38 to 28.80; see Hart, 1984 for definitions of these parameters). Notwithstanding the fact that their $^{87}Sr/^{86}Sr$ (0.70361 to 0.70369) and $^{143}Nd/^{144}Nd$ (0.51276 to 0.51279) ratios are clearly more and less radiogenic, respectively, than those observed for the Northern islands, the 2014 lavas plot on the second quadrant of the $^{87}Sr/^{86}Sr$ vs. $^{143}Nd/^{144}Nd$ diagram (Fig. 7A). This indicates a provenance from a time-integrated depleted source(s), i.e. which evolved over time with lower Rb/Sr and higher Sm/Nd than those of the BSE (bulk silicate earth) and the CHUR (chonditic uniform reservoir), respectively. Compared to the lavas extruded during the 1951 and 1995 eruptions, the 2014 rocks present more unradiogenic Sr and radiogenic Nd signatures (Fig. 7). The 2014 lavas also exhibit slightly more radiogenic $^{206}Pb/^{204}Pb$ ratios than the most samples from the two previous eruptions, the same being true for $^{207}Pb/^{204}Pb$ ratios (Fig. 6A). Lavas from these 3 eruptions are among the Cape Verde rocks with lower $^{206}Pb/^{204}Pb$ ratios. As is typical of the Southern Cape Verde Islands, rocks from these 3 eruptions are characterized by positive Δ8/4, plotting above the NHRL (Fig. 6B).

The 2014 lavas' $^{176}Hf/^{177}Hf$ ratios range from 0.28294 to 0.28296 (Table 2). A time-integrated evolution with high Lu/Hf ratios compared to CHUR is shown by positive εHf values (5.88 to 6.62; Fig. 7B), plotting between the mantle arrays proposed by Vervoort et al. (1999) and Chauvel et al. (2008). These are the first $^{176}Hf/^{177}Hf$ determinations available for Fogo Island, preventing any comparison with previous

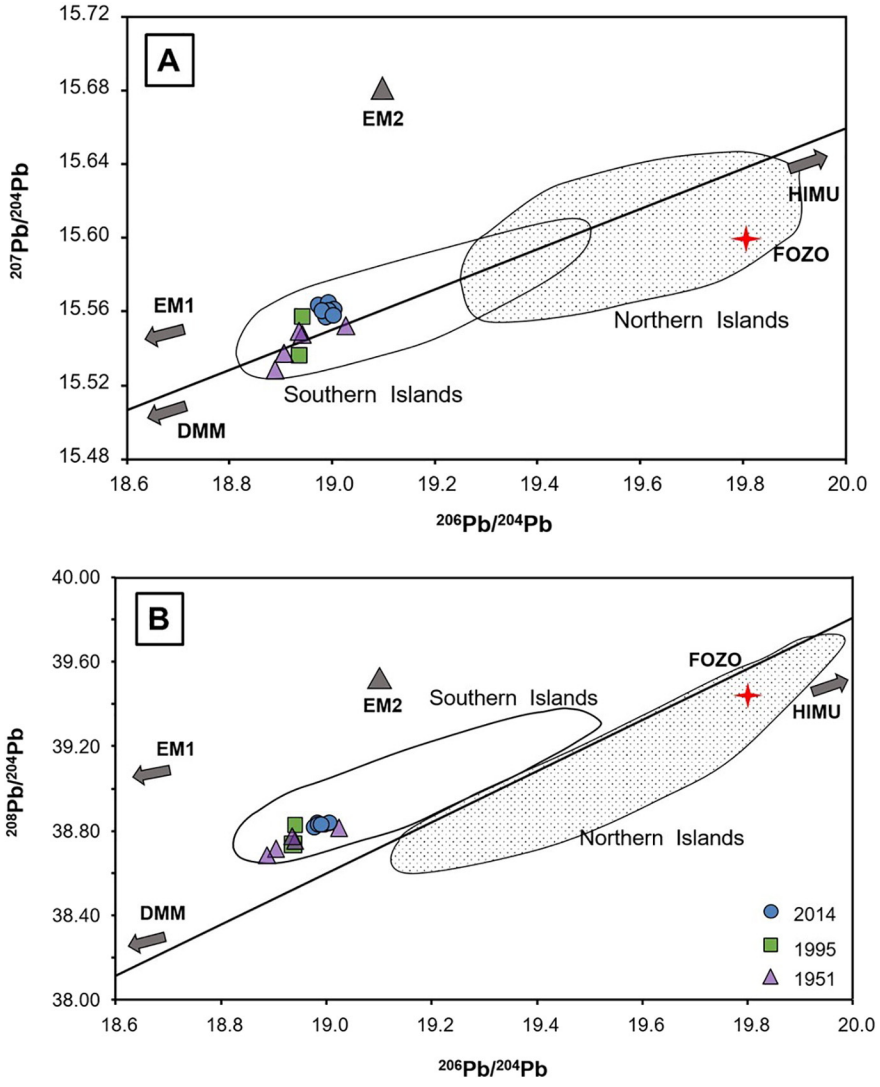

Fig. 6. Pb isotopic compositions (A: $^{206}Pb/^{204}Pb$ vs. $^{207}Pb/^{204}Pb$; B: $^{206}Pb/^{204}Pb$ vs. $^{208}Pb/^{204}Pb$). Data sources: Northern Islands (Santo Antão, São Vicente and São Nicolau: Holm et al., 2006; Jørgensen and Holm, 2002; Millet et al., 2008) and Southern Islands (Fogo and Santiago: Barker et al., 2010; Doucelance et al., 2003; Martins et al., 2010). The 1951 and 1995 eruptions data are from Escrig et al., 2005. The heavy line represents the Northern Hemisphere Reference Line (NHRL) defined by Hart (1984). Also plotted are the compositions of mantle components (see Iwamori and Nakamura, 2015).

results. However, it is noteworthy that the lavas erupted in 2014 plot inside the large field defined in the εNd-εHf space by the lavas from the neighbouring island of Santiago, which is characterized by significantly higher and lower $^{176}Hf/^{177}Hf$ ratios (see Barker et al., 2009; Martins et al., 2010). Significant correlations between any of these isotope signatures and ratios involving incompatible trace elements have not been found. This will be discussed later (see 5.3).

The $^{3}He/^{4}He$ ratio of a glassy phonotephrite was determined at the Institut de Physique du Globe de Paris (IPGP) using crushing for gas extraction. The obtained value (1.11 ± 0.13 Ra, where Ra is the present atmospheric ratio of 1.4×10^{-6}) for a ^{4}He concentration of 2.8×10^{-9} cm^3/g is interpreted as the result of atmospheric contamination during the eruption/consolidation of lava. Consequently, this result will not be considered in the discussion.

5. Discussion

5.1. Mantle source composition and magma evolution

Previous studies attributed the chemical variability of Fogo's lavas to a mixing of different proportions of HIMU-like (ancient recycled ocean crust) and EM1-like mantle end-members, diluted by the presence of depleted upper mantle (Gerlach et al., 1988) or by lower mantle material (Doucelance et al., 2003; Escrig et al., 2005) entrained by the upward moving plume.

Although the 2014 lavas present low $^{206}Pb/^{204}Pb$ ratios (up to 19.001), clearly below those typical of magmas originated from sources dominated by the HIMU mantle component (e.g. Kawabata et al., 2011), the HIMU fingerprint is shown by trace element patterns (Fig. 5) displaying enrichment in Nb and Ta relative to the LREE and the LILE (e.g. Niu et al., 2012). Additionally, all the analysed rocks are characterized by positive Δ8/4 and Δ7/4 and plot below the mixing lines between a HIMU type end-member and DMM or lower mantle compositions (Fig. 8), strongly suggesting the contribution of an EM1-type end-member to the 2014 Fogo mantle source(s). Interestingly, the products erupted in 2014 mark a change on the evolutionary trend reported by previous authors for Fogo eruptions (Escrig et al., 2005; Gerlach et al., 1988) which was characterized by an increasing contribution of the enriched component. Indeed, the 2014 lavas have less radiogenic Sr, but more radiogenic Nd signatures than those from the 1951 and 1995 eruptions.

Fogo's 2014 lavas (MgO ≤ 6.4 wt%, Mg# ≤ 53.2; Ni ≤ 42 ppm) cannot be considered representative of primary magmas. This fact and its chemical variability (MgO down to 2.93 wt.%; Ni down to 6 ppm)

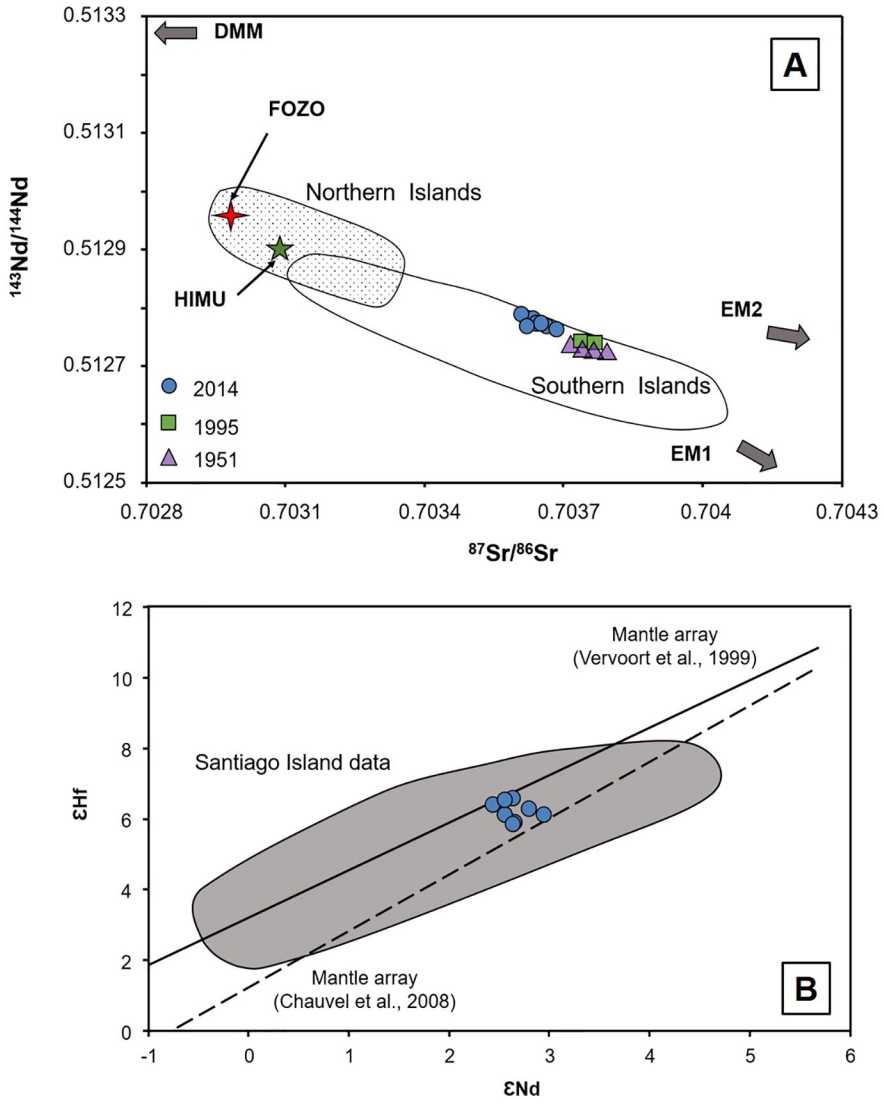

Fig. 7. Sr, Nd (A) and Hf (B) isotope compositions. Data sources: the Santiago Island field was defined using data from Barker et al. (2009) and Martins et al. (2010). See caption of Fig. 6 for further references. No Hf isotope data exist for the 1951 and 1995 eruptions.

emphasize the role of magma evolution processes to explain the observed compositional range. This is reinforced by the phonolitic composition of the glassy groundmass of some lavas (MgO down to 0.66 wt%; total alkalis up to 15.76 wt%; see Supplementary Material S3-G).

The important role of clinopyroxene fractionation is suggested by its occurrence as phenocryst in most samples and by the Sc decrease with increasing concentration of strongly incompatible trace elements such as La (Fig. 9A), here used as a proxy of magma evolution index. Fractionation of clinopyroxene must have been preceded by crystallization of olivine as indicated by the occurrence of olivine inclusions in clinopyroxene phenocrysts. The Dy/Dy* ratio, as defined by Davidson et al. (2013), tends to decrease from up to 0.81 in tephrites, down to 0.61 in phonotephrites, a tendency that, according to those authors, can be attributed either to amphibole or to clinopyroxene fractionation. If the importance of clinopyroxene fractionation was already demonstrated, the positive correlation of Dy/Dy* and Nb/U ratios (Fig. 9B) emphasizes the role of amphibole since, at odds with what happens with this mineral, clinopyroxene does not have the capacity to fractionate Nb from U (e.g. Adam and Green, 2006).

The calculated water content of the melt during kaersutite crystallization range from 3.81 to 4.14 wt% (±0.78 wt%), while oxygen fugacity is estimated in the range of 0.92 to 2.3 log units above NNO (±0.37 log units) using the methodology of Ridolfi and Renzulli (2012). The obtained fO_2 values are comparable to those reported for some other intraplate ocean islands (e.g. Madeira; Mata and Munhá, 2004). These relatively high fO_2 values are reflected in the composition of pyroxenes for which high Fe^{3+} contents were calculated based on the stoichiometry (Suplementary material S3-A), but not in the amphibole (Suplementary material S3-C). This suggests the incorporation of Ti (TiO_2 up to 6.13 wt%) into the octahedral position of kaersutite through the substitution $^{[VI]}R^{2+} + 2OH^- = {}^{[VI]}Ti^{4+} + 2O^{2-}$, which favours high Fe^{2+}/Fe^{3+} (Satoh et al., 2004).

As also reported for the previous Fogo's eruption (e.g. Hildner et al., 2012; Munhá et al., 1997) plagioclase did not play a significant role in the evolution of 2014 magmas. This is inferred from its rarity among phenocrysts and from the continuous Sr increase (1194 to 1408 ppm) throughout magma evolution. Judging from the comparatively high Al_2O_3, Na_2O and K_2O concentrations determined in the glassy phonolitic matrix, plagioclase and alkali feldspar fractionation was also not important for the generation of such evolved compositions. On the other hand, the role of Fe-Ti oxides and apatite fractionation is made evident by the significant decrease on P_2O_5 (Fig. 9C) and TiO_2 (not shown) concentrations from the most evolved tephrites (SiO_2 < 45.2.%) to phonotephrites (SiO_2 > 47.7 wt.%) (see also Table 1). The fractionation of these two non-

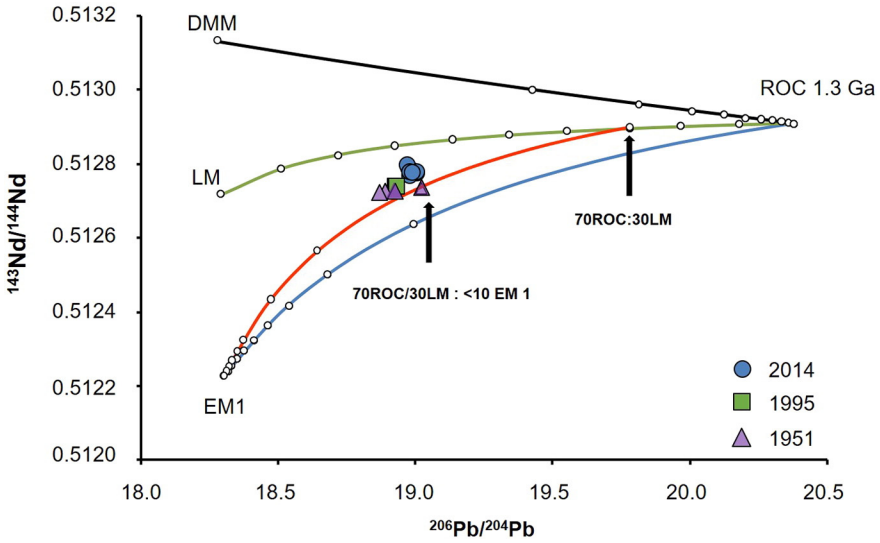

Fig. 8. The role of clinopyroxene, olivine, amphibole and apatite fractionation on the liquid lines of descent for the 2014, 1995 and 1951 eruptions. In 8A and 8B fractional crystallization was modelled using the Rayleigh equation. Partition coefficients used in calculations can be found in the Supplementary Material S5–1 and data relative to the fractional crystallization vectors in the S5–2. Circular ticks represent consecutive increments of 5% crystallization. Crystallization vectors corresponds to F = 0.7.

silicate phases, with the consequent significant increase in silica content of the residual magmatic liquids, was probably the cause for the small compositional gap ($\Delta SiO_2 = 2.5\%$) separating those two lithotypes.

Even though the isotope differences precludes the studied rocks to be considered comagmatic with those erupted in 1951 and 1995 (see Section 4.3), samples from these three eruptions plot along the same trends in most variation diagrams, suggesting that they share a common magma evolution history (e.g. Fig. 9 A and C). However, Fig. 9B emphasizes, despite similar trends, the lower Nb/U and Dy/Dy* ratios of the 2014 rocks relatively to the rocks of similar degree of evolution generated during the two previous eruptions.

Indeed, the less evolved 2014 rocks are characterized by lower Nb/U ratios (60 ± 3) than the basanitic/tephritic lavas from the 1995 and 1951 eruptions (95 ± 4; Hildner et al., 2011, 2012). Given the similar degree of evolution, these differences cannot be explained by fractional crystallization. The 2014 Nb/U ratios fit the typical OIB value (EM lavas excluded) of 52 ± 15 obtained by Hofmann (2003). As shown by this author, either the EM-type mantle components or the continental crust have significantly lower Nb/U ratios. Consequently the higher contribution of an enriched end-member (EM type) for the 1995 and 1951(see above) lavas cannot be invoked as a cause for their higher Nb/U ratios.

Nb/U ratios significantly higher than the typical OIB lavas have also been reported for some Canary lavas by Lundstrom et al. (2003). These authors defended that this can be the reflex of mixing between ascending plume-derived magmas and lithospheric melts with a significant contribution from amphibole present in low-solidus mantle domains. These domains would have been generated by metasomatic (s.l.) processes during previous stages of islands building. We suggest that a similar process may have been responsible for the significantly higher Nb/U and Dy/Dy* ratios of the 1995 and 1951 lavas. Since their vents, and probably also the ascending magma paths, were almost coincident with those of 2014, we speculate that such low-solidus lithospheric domains were already exhausted and did not contribute significantly for the composition of the subsequent 2014 eruption products.

As observed in the preceding 1995 eruption (Hildner et al., 2011; Munhá et al., 1997; Silva et al., 1997), the initial products erupted in 2014 were more evolved (phono-tephrites; SiO_2 up to 47.99 wt.%) than those emitted subsequently (tephrites, s.l.), for which SiO_2 contents as low as 43.03 wt.% were obtained. Considering the composition of the erupted magmas, assuming a complete degassing during eruption (suggested by very low loss on ignition), and using the algorithm of Giordano et al. (2008), the viscosity of the phonotephrites would have been some 10 times higher than that of the less evolved tephrites. This partially explains the evolution of lava flow morphology during the course of the eruption, which exhibited *a'a* characteristics during the initial eruptive stages, whilst *pāhoehoe* type lavas became more frequent during the subsequent effusion of the less viscous tephritic lava flows.

The temporal evolution of the erupted magma composition could result from the existence of a compositional/density zoning inside the pre-eruptive magma chamber. However, as proposed by Hildner et al. (2011) for the 1995 eruption, it probably indicates that magmas acquired their tephritic and phonotephritic compositions in separate magma reservoirs, as suggested by the low magmas viscosity and significant temperature differences (see below), both of which would favour magma mixing if they coexisted for a significant period.

5.2. Thermobarometric evidence for magma reservoirs into the mantle

Geothermobarometric estimates based on phenocrysts and cognate megacrysts have been considered to be important to constrain the magmatic plumbing system of a volcano, given that they can be used to calculate the depths of magma stalling/stagnation at mantle/crustal chambers. Indeed, silicates are characterized by very low intracrystalline diffusion rates, thus tending to preserve the composition acquired at the moment of crystallization.

We used the clinopyroxene-liquid thermobarometer of Putirka et al. (2003) for which lower uncertainties are foreseen than those reported for methods only using the clinopyroxene composition (Putirka, 2008; see also Geiger et al., 2016 for a review on clinopyroxene thermobarometry). The method is based on jadeite–diopside/hedenbergite exchange equilibria in hydrous conditions, which are shown to have existed at Fogo by the presence of amphibole (see also Section 5.1 for an estimate of water content in magma). As we used phenocryst cores and whole rock compositions as proxies of the crystal-liquid pairs, the P–T results obtained will be regarded as the conditions prevailing during early stages of clinopyroxene phenocrysts crystallization, assuming that no magma mixing occurred after pyroxene crystallization.

In order to use mineral/liquid thermobarometers it is mandatory to test if the crystal/melt pairs used testify equilibrium conditions. On a first approach a visual screening was made to identify textural evidence for disequilibrium, avoiding those showing irregular or reabsorbed

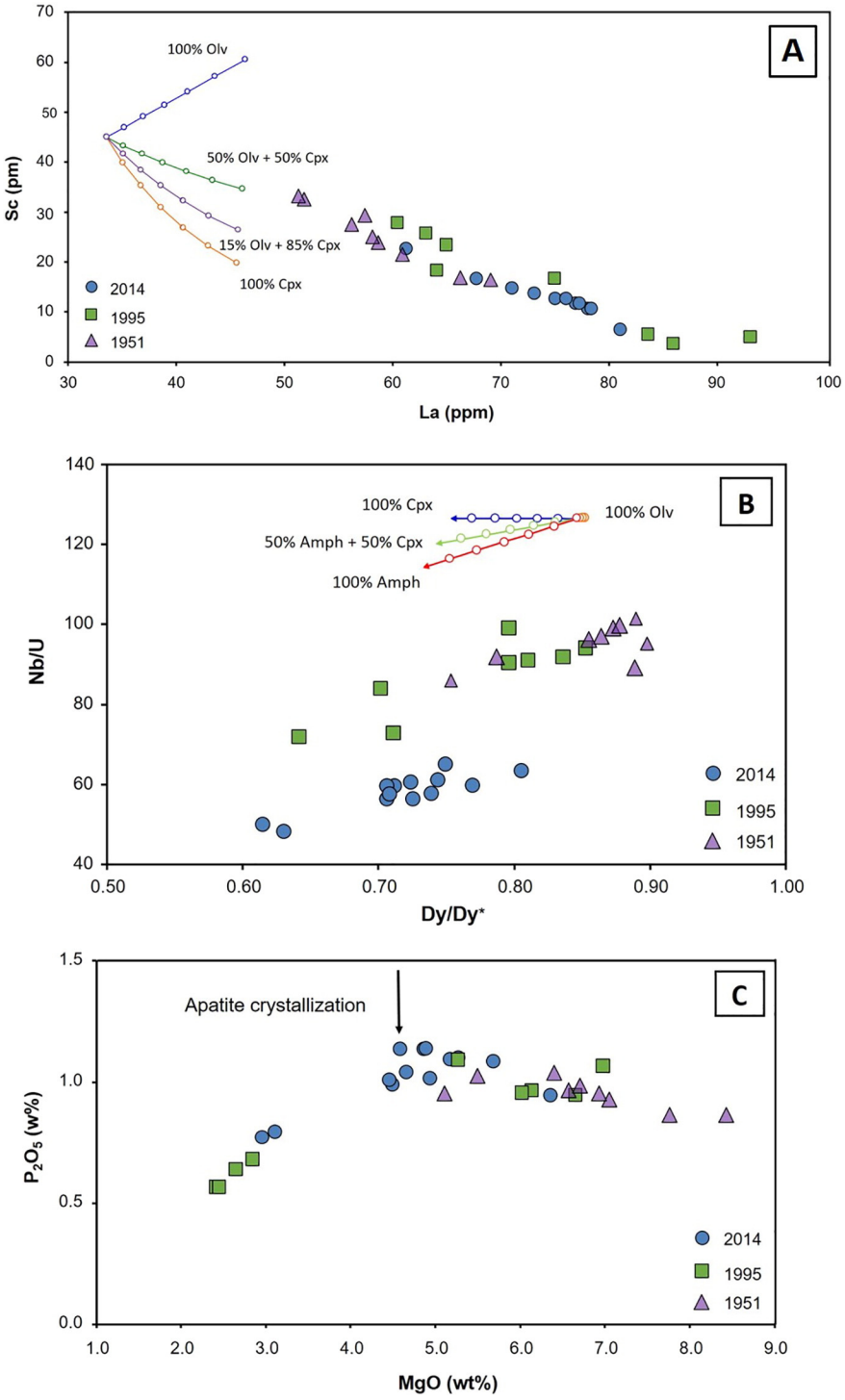

Fig. 9. Temperature and pressure conditions for crystallization of clinopyroxene and amphibole from the 2014 tephritic and phonotephritic magmas. Volcano not to scale. See main text for information about the uncertainties associated to thermobarometric determinations.

shapes. Furthermore, only core analyses of un-zoned or normally zoned phenocrysts where used. No mineral correction was made to the whole-rock composition due to the lack of evidence for significant accumulation (≤10% of phenocryst phases).

Considering the concerns regarding the efficacy of the Fe-Mg exchange in deciphering situations of pyroxene-melt equilibrium (e.g. Mollo et al., 2013), we used instead the comparison between predicted and measured components in clinopyroxene (diopside-hedenbergite; enstatite-ferrosilite; Ca-Tschermak's) as proposed by Putirka (1999). Following the recommendations of Putirka et al. (2003), only clinopyroxenes whose compositions are within the $\pm 2\sigma$ level of the predicted ones were used in the thermobarometric calculations. The standard errors of estimation (SEE) of the Putirka et al. (2003) method are 1.7 kbar and 33 °C, while analytical uncertainties, calculated using the relative standard deviation of whole rock and microprobe analyses of reference materials are significantly lower than the uncertainties of the method.

The temperatures obtained for pyroxene crystallization range from 1045 to 1063 °C for the phonotephrites and 1102 to 1143 °C for the tephrites. Pyroxene phenocrysts crystallized from phonotephritic

magmas at pressures in the range between 560 and 778 MPa, whereas the tephrites yield variations between 690 and 890 MPa (Fig. 10).

For amphiboles we used the single-phase thermobarometric and chemometric equations proposed by Ridolfi and Renzulli (2012), based on multivariate least-squares regression analyses of a large database of amphibole compositions in alkaline magma systems. For this method the authors claim low uncertainties: P ± 11.5%, T ± 23.5 °C. The application of the thermobarometer shows that the values obtained for kaersutites occurring in phonotephrites and tephrites are similar within error (1032 to 1050 °C and 568 to 620 MPa; see Fig. 9).

The kaersutite occurring in the 2014 Fogo lavas show ubiquitous signs for disequilibrium, presenting evidence for partial (reaction rims) to total (pseudomorphosis) substitution by polycrystalline aggregates of rhönite and clinopyroxene. We interpret the occurrence of rhönite and of the associated clinopyroxene as a consequence of the kaersutite destabilization resulting from magma degassing upon ascent, given the decrease of H_2O solubility in magmas as pressure drops (e.g. De Angelis et al., 2015). The destabilization of amphibole most probably occurs at pressures below 100–150 MPa (e.g., Rutherford, 2008) with reaction rims developing, for hornblende compositions, at pressures from circa 100 MPa down to 40 MPa (Browne and Gardner, 2006).

Amphibole reaction rims are often used to estimate magma ascent rate since their thickness and the size and shape of the replacing mineral phases are all dependent on it (Browne and Gardner, 2006; Chiaradia et al., 2011). Since the reaction rims observed in kaersutite crystals from the 2014 lavas are thick (>500 μm) and complete pseudomorphosis of mm-sized crystals (up to 4 mm) is common, it is valid to assume on a qualitative basis and based on Browne and Gardner's (2006) experimental data that the time of exposure of kaersutite to low PH_2O before quenching at the surface was >1 month, but < 50 days as suggested by seismic data (see below). Thus, the occurrence of rhönite and the degree of kaersutite replacement by rhönite suggest a late and short stagnation/stalling at crustal levels (i.e. at pressures below 100 MPa; <4.3 km below the island summit or <1.5 km below sea level) after a longer storage at deeper magma chambers.

In order to convert the calculated pressures to depths several assumptions has to be done, the depth of Moho being the one with more impact in the obtained results.

Vinnik et al. (2012), proposed that at the Cape Verde Archipelago the crust would be significantly thicker than the normal oceanic crust, extending down to 20–30 km depth. This was not supported by a later study (Wilson et al., 2013), which placed the Moho at significantly shallower depths, in agreement with the models of Lodge and Helffrich (2006), Pim et al. (2008) and Wilson et al. (2010). In this study we adopt 13.5 km as the depth of Moho beneath the Fogo Island (see Wilson et al., 2010; Wilson et al., 2013).

Considering a height of 5800 m for the Fogo island edifice (down to ≈3000 m below present sea level), an average density of 2400 $kg \cdot m^{-3}$ (Dash et al., 1976) for the island edifice, a crustal density of 2800 $kg \cdot m^{-3}$ inferred from seismic receiver functions (Lodge and Helffrich, 2006), a mantle density of about 3200 $kg \cdot m^{-3}$ at the Fogo region (Pim et al., 2008), a Moho depth at 13.5 km below sea level (Wilson et al., 2010; Wilson et al., 2013) and taking into account the uncertainties of the barometric methods (see above) the crystallization depth of clinopyroxene phenocrysts ranges approximately (±5.5 km) from 17.8 to 28.4 km below Fogo's summit, or 15.0 to 25.6 km below sea level. For amphiboles the same assumptions allow considering their crystallization at depths between 18.2 and 19.9 km (±3 km) below Fogo's summit, or 15.4 to 20.1 km below sea level. Considering the most common estimates for the crustal thickness at the Cape Verde region (≈12 to 13.5 km; Lodge and Helffrich, 2006; Pim et al., 2008; Wilson et al., 2010; Wilson et al., 2013) the obtained results suggest that the major fractionation events occurred in magma chambers located into the mantle.

Geobarometric studies of the previous two eruptions also revealed pre-eruptive magma storage at shallow mantle depths, followed by a short-period of magma stalling at crustal levels (Hildner et al., 2011,

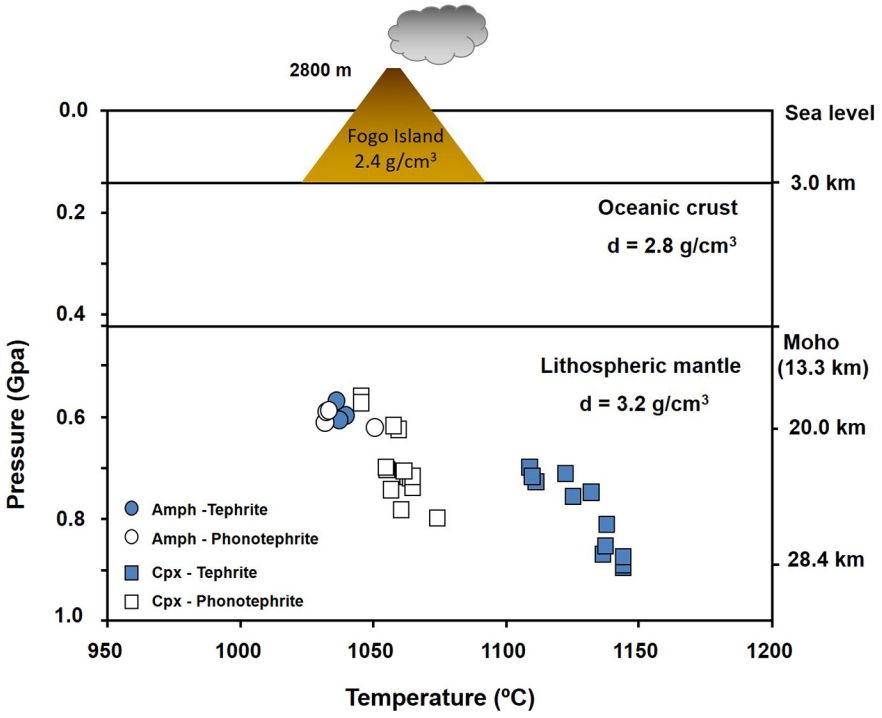

Fig. 10. Mixing model between depleted mantle (DMM) and recycled oceanic crust (ROC; ≈ HIMU), and between ROC and EM1and the lower mantle (LM). Values for these end-members are from Doucelance et al. (2003) (lower mantle), Iwamori and Nakamura (2015) (EM1, DMM) and Mourão et al. (2012a) (ROC). Given that the 2014 Fogo lavas are characterized by a diluted contribution of ROC (see main text), making difficult its constraint, we considered 1.3 Ga as the age of recycling for mixing calculations, as determined by Mourão et al. (2012a) for the neighbouring Brava Island. Additional line corresponds to a mixture between recycled oceanic crust and lower mantle material in a 60:40 proportion, with EM1. Circular marks represent 10% increments. See Supplementary Material S5–3 for mixing calculations.

2012; Munhá et al., 1997). The depths of clinopyroxene equilibration obtained in this study for the 2014 eruption (890 to 560 MPa; see above), although partially overlapping those presented for the historical eruptions by Hildner et al. (2011, 2012) (680 to 460 MPa), extends to higher pressures. However it must be noted that the pressure estimates by those authors refer to the final crystallization level, while our data represents the first crystallization stages of clinopyroxene phenocrysts.

The causes for the development of magma reservoirs within the mantle are still not well understood. Changes in buoyancy have been considered as an explanation for magma stagnation during ascent (e.g. Ryan, 1994). However, Jagoutz (2014) emphasized that ascending magmas can stagnate even when they are less dense than the surrounding rocks. A similar point of view was defended by Menand (2008) who considered that buoyancy is unlikely to be a major control in the emplacement of sills, which can be viewed as precursors of magma reservoirs (Gudmundsson, 2012). Moreover, as shown by Putirka (2017), hydrated magmas with MgO contents similar to those erupted in the 2014 Fogo eruption are less dense than the mantle, or even than the lower crustal rocks, indicating that buoyancy cannot be the explanation for the stagnation of Fogo magmas in the mantle. As proposed by Menand (2008), the presence of rheological anisotropies could be the primary factor determining the depth of magma stalling or stagnation. This can lead to the inference that the thickness of the elastic lithosphere exerts a major control on the depth of magma reservoirs. However, for the Cape Verde Archipelago the elastic thickness is estimated at 30 km (Pim et al., 2008) and our barometric data suggest magma emplacement at shallower depths, invalidating, in this case, such a proposal. Regional flexural stresses produced by the volcanic edifice loading are also thought to strongly influence the plumbing systems by generating a vertical contrast between tensile and compressive stress zones, capable of influencing the depth of magma stalling (see Putirka, 1997 and references therein). We do not have data to evaluate this hypothesis.

Whatever the cause for the development of mantle magma reservoirs, they seem to be common on ocean islands during periods of low magma supply rates (e.g. Klügel et al., 2015; Longpré et al., 2008; Stroncik et al., 2009) as was the case during the latest (this study) and the previous eruptions of Fogo volcano (Hildner et al., 2011, 2012; Munhá et al., 1997).

The scenario here proposed for the ascent of the 2014 Fogo magmas and of its plumbing system receives support from independent data. Indeed, a seismic event on October 4, 2014 (i.e. 50 days before the eruption) with a hypocentre 17 km below sea level (19.8 km below Fogo's summit), was interpreted by Instituto Nacional de Meteorologia e Geofísica (INMG, Cabo Verde) as resulting from the rupture of the roof of a mantle reservoir allowing magma transfer to shallower levels. Also, geodetic modelling of Sentinel-TOPS interferometry by González et al. (2015) revealed the lack of deformation at the island-scale during and pre-eruption times, further suggesting a deep location of the main magma reservoirs.

5.3. Evidence for small-scale mantle heterogeneity and short-term compositional evolution of Fogo volcano

As mentioned above, the Cape Verde Archipelago is known by its remarkable geochemical inter-island heterogeneity (e.g. Doucelance et al., 2003; Gerlach et al., 1988). Significant intra-island time-dependent geochemical variations are also common as shown for most Cape Verde Islands (e.g. Barker et al., 2010; Mourão et al., 2012a). Intra-island heterogeneities have also been described for presumably coeval rocks, such as the case of the Recent Volcanics of São Vicente Island (Trindade et al., 2003), and also of the Fogo Island where, as shown by Escrig et al. (2005), lavas erupted since 1785 present measurable variability on isotope signatures.

In opposition to incompatible trace-element ratios, which can be fractionated during partial melting and crystal fractionation processes, radiogenic isotope ratios are not changed during such events. They are thus a reliable indicator of source heterogeneity, even though the isotope variability of lavas tends to be smaller than that of the mantle source due to eventual mixing/homogenization processes (e.g. Stracke and Bourdon, 2009).

The 2014 volcanic products have clearly more unradiogenic Pb and Sr ($^{206}Pb/^{204}Pb$ down to 18.972; $^{87}Sr/^{86}Sr$ down to 0.703613) but more radiogenic Nd ($^{143}Nd/^{144}Nd$ up to 0.512789) signatures than the previous two eruptions ($^{206}Pb/^{204}Pb$ up to 19.273; $^{87}Sr/^{86}Sr$ up to 0.70379; $^{143}Nd/^{144}Nd$ down to 0.51272; see also Figs. 6 and 7). Considering that the 2014 lavas erupted from vents localized less than 200 and 2000 m of those from the two previous eruptions (1951 and 1995) and that these 3 eruptions occurred within a time lapse of only 63 years, such differences emphasize the presence of small-scale heterogeneities in the mantle sources feeding the volcanism of Fogo Island and the absence of significant magma mingling/homogenization before eruption.

The ability of magmas erupted from a volcano to show the source heterogeneity depends on the degree of partial melting, on the size of magma chambers and on the time of residence in these reservoirs. The higher the degree of partial melting, the higher is the capability of the extracted magmas to average the composition of a heterogeneous source. As a consequence low degree partial melts reflect better the compositional variability of the source (e.g. Martins et al., 2010; Stracke and Bourdon, 2009). It is accepted that the lithosphere exerts a major control in the final depth and extent of sub-lithospheric mantle melting (e.g. Haase, 1996; Humphreys and Niu, 2009; Niu et al., 2011; Watson and McKenzie, 1991). The extent of melting diminish with the increase of the lithosphere thickness, even though the thickness of mature (> 70 Ma) oceanic lithosphere tend to be constant, does not surpassing ≈90 km (Niu et al., 2011). The Cape Verde islands stand on a 120–140 My old oceanic crust characterized by significantly high values of admittance (geoid to depth ratio) (Monnereau and Cazenave, 1990). This suggests that lithosphere may extend to depths where garnet is the dominant aluminium-rich phase into the mantle (see Klemme and O'Neil, 2000; Ziberna et al., 2013) in agreement with previous studies for Cape Verde islands (e.g. Gerlach et al., 1988; Barker et al., 2010; Mourão et al., 2012a). Even taking into account that the less evolved 2014 magmas (tephrites) are not characterized by primary or primitive compositions, this percept is endorsed by (Tb/Yb)n ratios higher than 2.3, a value significantly above the threshold value of 1.8, above which garnet is considered more significant than spinel (Wang et al., 2002). Indeed it would be necessary to consider a (Tb/Yb)n increase higher than 27% during magma evolution – which is not expectable from the commonly accepted D values (e.g. Adam and Green, 2006) – to place the mean melting depths outside the garnet zone. Moreover, 2014 magmas show a Tb/Yb decrease from tephrites for the more evolved phonotephrites.

The thickness of the lithosphere exerts a first-order control on the extent of partial melting (e.g. Haase, 1996; Humphreys and Niu, 2009). For the present case, a lithosphere some 90 km thick (see above) would have constrained the melting to small extent. Despite the exact extent of melting being difficult to assess given the significantly evolved character of lavas (MgO < 6.4 wt%) and the uncertainty derived from the lack of knowledge about the relative proportion of peridotite and eclogite in the mantle source, the highly SiO_2 - undersaturated character of the Fogo lavas (2014: normative *ne* up to 23.04%) and the high TiO2 contents clearly suggest low percentages of partial melting, with the consequent deficient averaging of the isotopic variability of the source. The above referred lack of correlation between elemental and isotope ratios (see Section 4.3) also points to low degrees of melting during which a significant elemental fractionation occurs erasing any correlation between incompatible element ratios and isotope ratios (see Stracke and Bourdon, 2009).

After extraction, the degree of melt homogenization will depend on the presence of a plumbing system with large magmatic chamber(s), and of long magma residence times within the system, allowing mixing of different batches of melt. Data gathered from several islands suggest that for voluminous magma chambers to form, high magma supply

rates are needed; conversely, during evolutionary stages characterized by low magma supply rates a plethora of small and ephemeral magma reservoirs tend to form, many of them within the mantle (see Klügel et al., 2000, 2005; Stroncik et al., 2009 and references therein). Low eruption rates also characterized the 3 last Fogo´s eruptions here mentioned (1951, 1995 and 2014-15), with values < $15 m^3.s^{-1}$ being estimated for each of these volcanic events if pyroclasts are also included (see Madeira et al., 1997; Bagnardi et al., 2016; Richter et al., 2016; Siebert et al., 2010). This corresponds approximately to a mean eruption rate < 0.004 $km^3.yr^{-1}$, for the last 63 years, a value significantly lower than those reported for the contemporary Kilauea activity (at least 0.1 $km^3.yr^{-1}$) where shallow magma chambers feed the volcanism (Poland et al., 2014). The evidence for small and ephemeral magma reservoirs beneath Fogo was already proposed for the previous eruptions (Hildner et al., 2012; Munhá et al., 1997). This may be also the case for the 2014 eruption as suggested by the compositional change of lavas (from phonotephrites to basanites/tephrites) and, despite the errors associated with barometric methods, by distinct depths of magma chambers inferred from clinopyroxene and kaersutite phenocrysts and cognate megacrysts. This plumbing system, limiting magma mixing/homogenization, contributed to the preservation of the heterogeneities inherited from the mantle source.

6. Concluding remarks

- Magmas erupted from November 23 to December 7, 2014 at Fogo Island (Cape Verde Archipelago) are alkaline, exhibit significantly evolved compositions (Ni < 42 ppm) and are classified as tephrites and phonotephrites. The compositional range is slightly smaller than that reported for the 1995 eruption, but larger than the displayed by the 1951 eruption, during which no phonotephrites were erupted.
- Similarly to 1995 (Hildner et al., 2011; Munhá et al., 1997; Silva et al., 1997), the eruption of phonotephritic lavas preceded the effusion of the tephritic ones suggesting, in agreement with barometric data, the existence of several magma reservoirs. The occurrence of a compositional/density zoning inside the pre-eruptive magma chamber cannot be completely excluded.
- Geobarometric estimates using clinopyroxene and kaersutite compositions indicate that fractional crystallization mainly occurred in magma chambers located in the mantle (down to 25.6 ± 5.5 km below the sea level), followed by a short residence time (≈50 days) at crustal levels.
- Erupted magmas are characterized by positive εNd, εHf, Δ8/4 and Δ7/4. Their compositions reflect a mantle source where ancient recycled ocean crust and an enriched component (EM1-type) are present. The 2014 lavas have less radiogenic Sr, but more radiogenic Nd compositions, than those from the 1951 and 1995 eruptions, marking a change on the evolutionary trend reported by previous authors for Fogo (Escrig et al., 2005; Gerlach et al., 1988) which was characterized by an increasing contribution of the EM1-type component.
- Although the 2014 eruption vents are almost spatially coincident with those of 1995 and less than 2 km away from the 1951 vents, their lavas are isotopically different from those generated in the previous two eruptions. These differences in magmas erupted on a very limited area and short interval (63 years) reflect the heterogeneity of the mantle source and the lack of averaging/mingling during partial melting and ascent through the plumbing system. For these, the lid effect of the old (120–140 Ma) and thick lithosphere is considered of utmost importance.
- The lower Nb/U ratios of the 2014 rocks as compared with previous eruptions is considered to reflect the lack of significant mixing of ascending plume magmas with lithospheric melts, as opposed to what has been hypothesised for 1995 and 1951 magmas.

Supplementary data to this article can be found online at http://dx.doi.org/10.1016/j.lithos.2017.07.001.

Acknowledgements

We dedicate this paper to the memory of Luís Celestino Silva (1936-2017), a pioneer in the geology of Cape Verde: his knowledge, enthusiasm and kindness marked most of the authors of this work.

This research received financial support from FCT (Fundação para a Ciência e Tecnologia) through projects REGENA (PTDC /GEO-FIQ/3648/2012) and FIRE (PTDC/GEO-GEO/1123/2014), as well as through project UID/GEO/50019/2013 to Instituto Dom Luiz (IDL). R. Ramalho was funded by a FP7-PEOPLE-2011-IOF Marie Curie International Outgoing Fellowship, which is acknowledged. The authors are grateful to Pedro Rodrigues for skilled assistance during electron microprobe analyses. J. Mata did not receive financial support from C4G. His field work was funded by Centro de Geologia da Universidade de Lisboa and Bernardo Mata. Kayla Iacovino is acknowledged for the permission to use her Excel spreadsheet to calculate magma viscosity (see http://www.kaylaiacovino.com/tools-for-petrologists/). Cristina de Ignacio, an anonymous reviewer and the Editor (Nelson Eby) are acknowledged for their constructive comments, corrections and suggestions, which significantly contributed for the quality of this paper.

References

Adam, J., Green, T., 2006. Trace element partitioning between mica and amphibole-bearing garnet lherzolite and hydrous basanitic melt: 1. Experimental results and the investigation of controls on partitioning behavior. Contributions to Mineralogy and Petrology 152, 1–17.

Bagnardi, M., Gonzàlez, P.J., Hooper, A., 2016. High-resolution digital elevation model from tri-stereo Pleiades-1 satellite imagery for lava flow volume estimates at Fogo volcano: tri-stereo Pleiades DEM of Fogo volcano. Geophysical Research Letters 43. http://dx.doi.org/10.1002/2016GL06945.

Barker, A.K., Holm, P.M., Peate, D.W., Baker, J.A., 2009. Geochemical stratigraphy of submarine lavas (3–5 Ma) from the Flamengos Valley, Santiago, southern Cape Verde islands. Journal of Petrology 50, 169–193.

Barker, A.K., Holm, P.M., Peate, D.W., Baker, J.A., 2010. A 5 million year record of compositional variations in mantle sources to magmatism on Santiago, southern Cape Verde archipelago. Contributions to Mineralogy and Petrology 160, 133–154.

Barker, A.K., Troll, V.R., Ellam, R.M., Hansteen, T.H., Harris, C., Stillman, C.J., Andersson, A., 2012. Magmatic evolution of the Cadamosto seamount, Cape Verde: beyond the spatial extent of EM1. Contributions to Mineralogy and Petrology 163, 949–965.

Beier, C., Haase, K.M., Abouchami, W., Krienitz, M.-S., Hauff, F., 2008. Magma genesis by rifting of oceanic lithosphere above anomalous mantle: Terceira rift, Azores. Geochemistry, Geophysics, Geosystems 9, Q12013.

Browne, B.L., Gardner, J.E., 2006. The influence of magma ascent path on the texture, mineralogy, and formation of hornblende reaction rims. Earth and Planetary Science Letters 246, 161–176.

Brum da Silveira, A., Madeira, J., Munhá, J., Mata, J., Martins, S., Mourão, C., Tassinari, C., 2006. The summit depression of Fogo Island (Cape Verde): caldera and/or flank collapse? Abstracts and Programme of the George P. L. Walker Symposium on Advances in Volcanology, Reykolt, Islândia, p. 23

Caldeira, R., Guimarães, F., Mata, J., Silva, P., Moreira, M., Ferreira, P., 2015. Mineral chemistry of ultramafic nodules from lavas of the Fogo Island 2014 eruption (Cape Verde). Preliminary results. Livro de Resumos do X Congresso Ibérico de Geoquímica/XVIII Semana de Geoquímica. LNEG, Lisboa, pp. 51–53.

Cappello, A., Ganci, G., Calvari, S., Pérez, N.M., Hernández, P.A., Silva, S.V., Cabral, J., Del Negro, C., 2016. Lava flow hazard modeling during the 2014–2015 Fogo eruption, Cape Verde. Journal of Geophysical Research, Solid Earth 121, 1–14.

Cashman, K.V., Sparks, R.S.J., Blundy, J.D., 2017. Vertically extensive and unstable magmatic systems: a unified view of igneous processes. Science 355, eaag3055 (9 pages).

Chauvel, C., Blichert-Toft, J., 2001. A hafnium isotope and trace element perspective on melting of the depleted mantle. Earth and Planetary Science Letters 190, 137–151.

Chauvel, C., Lewin, E., Carpentier, M., Arndt, N., Marini, J.-C., 2008. Role of recycled oceanic basalt and sediment in generating the Hf–Nd mantle array. Nature Geoscience 1, 64–67.

Chauvel, C., Bureau, S., Poggi, C., 2011. Comprehensive chemical and isotopic analyses of basalt and sediment reference materials. Geostandards and Geoanalytical Research 35, 125–143.

Chiaradia, M., Müntener, O., Beate, B., 2011. Enriched basaltic andesites from mid-crustal fractional crystallization, recharge, and assimilation (Pilavo Volcano, Western Cordillera of Ecuador). Journal of Petrology 52, 1107–1141.

Christensen, B., Holm, P., Jambon, A., Wilson, J., 2001. Helium, argon and lead isotopic composition of volcanics from Santo Antão and Fogo, Cape Verde Islands. Chemical Geology 178, 127–142.

Cooper, K.M., 2017. What does a magma reservoir look like? The "crystal's eye" view. Elements 13, 23–28.

Courtney, R., White, R., 1986. Anomalous heat flow and geoid across the Cape Verde rise: evidence for dynamic support from a thermal plume in the mantle. Geophysical Journal of the Royal Astronomical Society 87, 815–868.

Dash, B.P., Ball, M.M., King, G.A., Butler, I.W., Rona, P.A., 1976. Geophysical investigation of the Cape Verde archipelago. Journal of Geophysical Research 81, 5249–5259.

Davidson, J., Turner, S., Plank, T., 2013. Dy/Dy*: variations arising from mantle sources and petrogenetic processes. Journal of Petrology 54, 525–537.
Day, S., Heleno da Silva, S., Fonseca, J., 1999. A past giant lateral collapse and present day instability of Fogo, Cape Verde Islands. Journal of Volcanology and Geothermal Research 94, 191–218.
De Angelis, S.H., Larsen, J., Coombs, Dunn, A., Hayden, L., 2015. Amphibole reaction rims as a record of pre-eruptive magmatic heating: an experimental approach. Earth and Planetary Science Letters 426, 235–245.
Doucelance, R., Escrig, S., Moreira, M., Gariépy, C., Kurz, M.D., 2003. Pb-Sr-He isotope and trace element geochemistry of the Cape Verde archipelago. Geochimica et Cosmochimica Acta 67, 3717–3733.
Eisele, S., Reißig, S., Freundt, A., Kutterolf, S., Nürnberg, D., Wang, K.L., Kwasnitschka, T., 2015. Pleistocene to Holocene offshore tephrostratigraphy of highly explosive eruptions from the southwestern Cape Verde archipelago. Marine Geology 369, 233–250.
Escrig, S., Doucelance, R., Moreira, M., Allègre, C.J., 2005. Os isotope systematics in Fogo Island: evidence for lower continental crust fragments under the Cape Verde southern islands. Chemical Geology 219, 93–113.
Faria, B., Fonseca, J.F.B.D., 2014. Investigating volcanic hazard in Cape Verde Islands through geophysical monitoring: network description and first results. Natural Hazards and Earth System Sciences 14, 485–499.
Foeken, J.P.T., Day, S., Stuart, F.M., 2009. Cosmogenic ^{3}He exposure dating of the quaternary basalts from Fogo, cape Verdes: implications for rift zone and magmatic reorganisation. Quaternary Geochronology 4, 37–49.
Forte, A.M., Quere, S., Moucha, R., Simmons, N.A., Grand, S.P., Mitrovica, J.X., Rowley, D.B., 2010. Joint seismic-geodynamic-mineral physical modelling of African geodynamics: a reconciliation of deep-mantle convection with surface geophysical constraints. Earth and Planetary Science Letters 295, 329–341.
French, S.W., Romanowicz, B., 2015. Broad plumes rooted at the base of the earth's mantle beneath major hotspots. Nature 525, 95–99.
Galer, S.J.G., Abouchami, W., 1998. Pratical application of lead triple spiking for correction of instrumental mass discrimination. Mineralogical Magazine 62 (A), 491–492.
Geiger, H., Barker, A., Troll, V., 2016. Locating the depth of magma supply for volcanic eruptions, insights from Mt. Cameroon. Scientific Reports 6, 33629.
Gerlach, D., Cliff, R., Davies, G., Norry, M., Hodgson, N., 1988. Magma sources of the Cape Verde archipelago: isotopic and trace element constraints. Geochimica et Cosmochimica Acta 52, 2979–2992.
Gibson, S.A., Geist, D.G., Day, J.A., Dale, C.W., 2012. Short wavelength heterogeneity in the Galápagos plume: evidence from compositionally diverse basalts on Isla Santiago. Geochemistry, Geophysics, Geosystems 13. http://dx.doi.org/10.1029/2012GC004244.
Giordano, D., Russell, J.K., Dingwell, D.B., 2008. Viscosity of magmatic liquids: a model. Earth and Planetary Science Letters 217, 123–134.
González, P.J., Bagnardi, M., Hooper, A.J., Larsen, Y., Marinkovic, P., Samsonov, S.V., Wright, T.J., 2015. The 2014–2015 eruption of Fogo volcano: geodetic modeling of sentinel-1 TOPS interferometry. Geophysical Research Letters 42, 9239–9246.
Gudmundsson, A., 2012. Magma chambers: formation, local stresses, excess pressures, and compartments. Journal of Volcanology and Geothermal Research 237–238, 19–41.
Haase, K.M., 1996. The relationship between the age of the lithosphere and the composition of oceanic magmas: constraints on partial melting, mantle sources and the thermal structure of the plates. Earth and Planetary Science Letters 144, 75–92.
Hart, S.R., 1984. A large-scale isotope anomaly in the southern hemisphere mantle. Nature 309, 753–757.
Hildner, H., Klügle, A., Hauff, F., 2011. Magma storage and ascent during the 1995 eruption of Fogo, Cape Verde archipelago. Contributions to Mineralogy and Petrology 162, 751–772.
Hildner, H., Klügle, A., Hansteen, T., 2012. Barometry of lavas from 1951 eruption of Fogo, Cape Verde Islands: implications for historic and prehistoric magma plumbing system. Journal of Volcanology and Geothermal Research 217-218, 73–90.
Hoernle, K., Tilton, G., Le Bas, M.J., Duggen, S., Garbe-Schönberg, D., 2002. Geochemistry of oceanic carbonatites compared with continental carbonatites: mantle recycling of oceanic crustal carbonate. Contributions to Mineralogy and Petrology 142, 520–542.
Hofmann, A.W., 2003. Sampling mantle heterogeneity trough oceanic basalts: isotopes and trace elements. In: Carlson, R. (Ed.), Treatise on Geochemistry. The mantle and core vol. 2. Elsevier-Pergamon, Oxford, pp. 61–101.
Holm, P.M., Wilson, J.R., Christensen, B.P., Hansen, L., Hansen, S.L., Hein, K.M., Mortensen, A.K., Pedersen, R., Plesner, S., Runge, M.K., 2006. Sampling the Cape Verde mantle plume: evolution of the melt compositions on Santo Antão, Cape Verde Islands. Journal of Petrology 47, 145–189.
Holm, P.M., Grandvuinet, T., Friis, J., Wilson, J.R., Barker, A.K., Plesner, S., 2008. An ^{40}Ar-^{39}Ar study of the Cape Verde hot spot: temporal evolution in a semistationary plate environment. Journal of Geophysical Research 113, B08201.
Humphreys, E., Niu, Y., 2009. On the composition of ocean island basalts (OIB): the effects of lithospheric thickness variation and mantle metasomatism. Lithos 112, 118–136.
Iwamori, H., Nakamura, H., 2015. Isotopic heterogeneity of oceanic, arc and continental basalts and its implications for mantle dynamics. Gondwana Research 27, 1131–1152.
Jagoutz, O., 2014. Arc crustal differentiation mechanisms. Earth and Planetary Science Letters 396, 67–77.
Jørgensen, J.Ø., Holm, P.M., 2002. Temporal variation and carbonatite contamination in primitive ocean island volcanics from S. Vicente, Cape Verde Islands. Chemical Geology 192, 249–267.
Kawabata, H., Hanyu, T., Chang, Q., Kimura, J., Nichols, A.R.L., Tatsumi, Y., 2011. The petrology and geochemistry of St. Helena alkali basalts: evaluation of the oceanic crust-recycling model for HIMU OIB. Journal of Petrology 52, 791–838.
Klemme, S., O'Neil, H., 2000. The near solidus transition from garnet lherzolite to spinel lherzolite. Contributions to Mineralogy and Petrology 138, 237–248.
Klügel, A., Hoernle, K.A., Schmincke, H.-U., White, J.D.L., 2000. The chemically zoned 1949 eruption on La Palma (Canary Islands): petrologic evolution and magma supply dynamics of a rift-zone eruption. Journal of Geophysical Research 105, 5997–6016.
Klügel, A., Hansteen, T.H., Galipp, K., 2005. Magma storage and underplating beneath Cumbre Vieja volcano, La Palma (Canary Islands). Earth and Planetary Science Letters 236, 211–226.
Klügel, A., Longpré, M.-A., Cañada, L.C., Stix, J., 2015. Deep intrusions, lateral magma transport and related uplift at ocean island volcanoes. Earth and Planetary Science Letters 431, 140–149.
Kogarko, L.N., Asavin, A.M., 2007. Regional features of primary alkaline magmas of the Atlantic Ocean. Geochemistry International 45, 841–856.
Le Bas, M., 1989. Nephelinitic and basanitic rocks. Journal of Petrology 30, 1299–1312.
Le Maitre, R.W., 2002. . Igneous Rocks: A Classification and Glossary of Terms, Recommendations of the International Union of Geological Sciences, Subcommission of the Systematics of Igneous Rocks. In: Streckeisen, A., Zanettin, B., Le Bas, M.J., Bonin, B., Bateman, P., Bellieni, G., Dudek, A., Efremova, S., Keller, J., Lameyre, J., Sabine, P.A., Schmid, R., Sorensen, H., Woolley, A.R. (Eds.), Cambridge University Press. ISBN: 0-521-66215-X.
Liu, X., Zhao, D., 2014. Seismic evidence for a mantle plume beneath the Cape Verde hotspot. International Geology Review 56, 1213–1225.
Lodge, A., Helffrich, G., 2006. Depleted swell root beneath the Cape Verde Islands. Geology 34, 449–452.
Longpré, M., Troll, V.R., Hansteen, T.H., 2008. Upper mantle magma storage and transport under a Canarian shield-volcano, Teno, Tenerife (Spain). Journal of Geophysical Research 113. http://dx.doi.org/10.1029/2007JB005422.
Lundstrom, C.C., Hoernle, K., Gill, J., 2003. U-series disequilibria in volcanic rocks from the Canary Islands: plume versus lithospheric melting. Geochimica et Cosmochimica Acta 67, 4153–4177.
MacDonald, G.A., 1968. Composition and origin of Hawaiian lavas. Geological Society of America Memoirs 116, 477–522.
Madeira, J., Brum da Silveira, A., Torres, P.C., 1997. A erupção vulcânica de 1995 na Ilha do Fogo, Cabo Verde. In: Réffega, A., Figueiredo, M., Silva, L., Costa, F., Mendes, M., Torres, P., Silva, T., Correia, E. (Eds.), IICT, Lisboa, pp. 153–163.
Madeira, J., Munhá, J., Tassinari, C., Mata, J., Brum, A., Martins, S., 2005. K/Ar ages of carbonatites from the Island of Fogo (Cape Verde). VIII Congresso Ibérico de Geoquímica e XIV Semana de Geoquímica (Portugal).
Madeira, J., Brum da Silveira, A., Mata, J., Mourão, C., Martins, S., 2008. The role of mass movements on the geomorphologic evolution of ocean islands: examples from Fogo and Brava in the Cape Verde archipelago. Comunicações Geológicas 95, 99–112.
Madeira, J., Mata, J., Mourão, C., Brum da Silveira, A., Martins, S., Ramalho, R., Hoffmann, D.L., 2010. Volcano-stratigraphic and structural evolution of Brava Island (Cape Verde) based on ^{40}Ar/^{39}Ar, U–Th and field constraints. Journal of Volcanology and Geothermal Research 196, 219–235.
Madureira, P., Mata, J., Mattielli, N., Queiroz, G., Silva, P., 2011. Mantle source heterogeneity, magma generation and magmatic evolution at Terceira Island (Azores archipelago): constraints from elemental and isotopic (Sr, Nd, Hf, and Pb) data. Lithos 126, 402–418.
Martins, S., Mata, J., Munhá, J., Mendes, M.H., Maerschalk, C., Caldeira, R., Mattielli, N., 2010. Chemical and mineralogical evidence of the occurrence of mantle metasomatism by carbonate-rich melts in an oceanic environment (Santiago Island, Cape Verde). Mineralogy and Petrology 99, 43–65.
Masson, D.G., Le Bas, T.P., Grevemeyer, I., Weinrebe, W., 2008. Flank collapse and large-scale landsliding in the Cape Verde Islands, off West Africa. Geochemistry, Geophysics, Geosystems 9 (7).
Mata, J., Munhá, J., 2004. Madeira Island alkaline lava spinels: petrogenetic implications. Mineralogy and Petrology 81, 85–111.
Mata, J., Moreira, M., Doucelance, R., Ader, M., Silva, L.C., 2010. Noble gas and carbon isotopic signatures of Cape Verde oceanic carbonatites: implications for carbon provenance. Earth and Planetary Science Letters 291, 70–83.
Menand, T., 2008. The mechanics and dynamics of sills in elastic layered media and their implications for the growth of laccoliths. Earth and Planetary Science Letters 267, 93–99.
Millet, M.A., Doucelance, R., Schiano, P., David, K., Bosq, C., 2008. Mantle plume heterogeneity versus shallow-level interactions: a case study, the São Nicolau Island, Cape Verde archipelago. Journal of Volcanology and Geothermal Research 176, 265–276.
Mollo, S., Putirka, K., Misiti, V., Soligo, M., Scarlato, P., 2013. A new test for equilibrium based on clinopyroxene-melt pairs: clues on the solidification temperatures of Etnean alkaline melts at post-eruptive conditions. Chemical Geology 352, 92–100.
Monnereau, M., Cazenave, A., 1990. Depth and geoid anomalies over oceanic hotspot swells: a global survey. Journal of Geophysical Research (Solid Earth) 95, 15–429.
Montelli, R., Nolet, G., Dahlen, F.A., Masters, G., 2006. A catalogue of deep mantle plumes: new results from finite-frequency tomography. Geochemistry, Geophysics, Geosystems 7. http://dx.doi.org/10.1029/2006GC001248.
Mourão, C., Mata, J., Doucelance, R., Madeira, J., Millet, M.-A., Moreira, M., 2012a. Geochemical temporal evolution of Brava Island magmatism: constraints on the variability of Cape Verde mantle sources and on the carbonatite-silicate magma link. Chemical Geology 334, 44–61.
Mourão, C., Moreira, M., Mata, J., Raquin, A., Madeira, J., 2012b. Primary and secondary processes constraining the noble gas isotopic signatures of carbonatites and silicate rocks from Brava Island: evidence for a lower mantle origin of the Cape Verde plume. Contributions to Mineralogy and Petrology 163, 995–1009.
Munhá, J.M., Mendes, M.H., Palácios, T., Silva, L.C., Torres, P.C., 1997. Petrologia e geoquímica da erupção de 1995 e de outras lavas históricas da ilha do Fogo, Cabo Verde. In: Réffega, A., et al. (Eds.), A Erupção Vulcânica de 1995 na Ilha do Fogo, Cabo Verde. IICT, Lisboa, pp. 171–186.

Niu, Y., Wilson, M., Humphreys, E.R., O'Hara, M.J., 2011. The origin of intra-plate ocean island basalts (OIB): the lid effect and its geodynamic implications. Journal of Petrology 52, 1443–1468.
Niu, Y.L., Wilson, M., Humphreys, E.R., O'Hara, M.J., 2012. A trace element perspective on the source of ocean island basalts (OIB) and fate of subducted ocean crust (SOC) and mantle lithosphere (SML). Episodes 35, 310–327.
Nobre Silva, I., Weis, D., Scoates, J., 2013. Isotopic systematics of the early Mauna Kea shield phase and insight into the deep mantle beneath the Pacific Ocean. Geochemistry, Geophysics, Geosystems 11, Q 09011. http://dx.doi.org/10.1029/2010gc003176.
Palme, H., O'Neil, H.S.C., 2003. Cosmochemical estimates of mantle compositions. In: Carlson, R. (Ed.), The Mantle and Core. Treatise on Geochemistry vol. 2, pp. 1–38.
Paris, R., Giachetti, T., Chevalier, J., Guillou, H., Frank, N., 2011. Tsunami deposits in Santiago Island (Cape Verde archipelago) as possible evidence of a massive flank failure of Fogo volcano. Sedimentary Geology 239, 129–145.
Pim, J., Peirce, C., Watts, A.B., Grevemeyer, I., Krabbenhoeft, A., 2008. Crustal structure and the origin of the Cape Verde rise. Earth and Planetary Science Letters 272, 422–428.
Poland, M.P., Miklius, A., Montgomery-Brown, E.K., 2014. Magma supply, storage, and transport at shield-stage Hawaiian volcanoes. In: Poland, M.P., Takahashi, T.J., Landowski, C.M. (Eds.), Characteristics of Hawaiian Volcanoes. U.S. Geological Survey Professional Paper 1801, 179–234.
Pollitz, F., 1991. Two-stage model of African absolute motion during the last 30 million years. Tectonophysics 194, 91–106.
Putirka, K., 1997. Magma transport at Hawaii: inferences based on igneous thermobarometry. Geology 25, 69–72.
Putirka, K., 1999. Clinopyroxene + liquid equilibria to 100 kbar and 2450 K. Contributions to Mineralogy and Petrology 135, 151–163.
Putirka, K.D., 2008. Thermometers and barometers for volcanic systems. Reviews in Mineralogy and Geochemistry 69, 61–120.
Putirka, K.D., 2017. Down the crater: where magmas are stored and why they erupt. Elements 13, 11–16.
Putirka, K., Mikaelian, H., Ryerson, F., Shaw, H., 2003. New clinopyroxene-liquid thermobarometers for mafic, evolved, and volatile-bearing lava compositions, with applications to lavas from Tibet and the Snake River Plain, Idaho. American Mineralogist 88, 1542–1554.
Ramalho, R., 2011. Building the Cape Verde Islands. Springer Theses (207 pp.).
Ramalho, R., Helffrich, G., Cosca, M., Vance, D., Hoffmann, D., Schmidt, D.N., 2010. Episodic swell growth inferred from variable uplift of the Cape Verde hotspot islands. Nature Geoscience 3, 774–777.
Ramalho, R., Winckler, G., Madeira, J., Helffrich, G., Hipólito, A., Quartau, R., Adena, K., Schaefer, J., 2015. Hazard potential of volcanic flank collapses raised by new megatsunami evidence. Science Advances 1. http://dx.doi.org/10.1126/sciadv.1500456.
Ribeiro, O., 1954. A ilha do Fogo e as suas erupções. Junta de Investigações do Ultramar, Memórias, Série Geográfica I, Lisboa.
Richter, N., Favalli, M., Dalfsen, E.Z., Fornaciai, A., Fernandes, R.M.S., Rodriguez, N.P., Levy, J., Victória, S.S., Walter, Th.R., 2016. Lava flow hazard at Fogo volcano, Cape Verde, before and after the 2014–2015 eruption. Natural Hazards and Earth Systems 16, 1925–1951.
Ridolfi, F., Renzulli, A., 2012. Calcic amphiboles in calc-alkaline and alkaline magmas: thermobarometric and chemometric empirical equations valid up to 1130 °C and 2.2 GPa. Contributions to Mineralogy and Petrology 163, 877–895.
Rutherford, M.J., 2008. Magma ascent rates. In: Putirka, K.D., Tepley III, F.J. (Eds.), Minerals, Inclusions and Volcanic Processes. Mineralogical Society of America and Geochemical Society Reviews, in Mineralogy and Geochemistry vol. 69, pp. 241–271.
Ryan, M., 1994. Neutral-buoyancy controlled magma transport and storage in mid-ocean ridge magma reservoirs and their sheeted-dike complex: a summary of basic relationships. In: Ryan, M.P. (Ed.), Magmatic Systems. Academic, San Diego, Caliornia (Chap. 6).
Saki, M., Thomas, C., Nippress, S.E.J., Lessing, S., 2015. Topography of upper mantle seismic discontinuities beneath the North Atlantic: the Azores, Canary and Cape Verde plumes. Earth and Planetary Science Letters 409, 193–202.
Satoh, H., Yamaguchi, Y., Makino, K., 2004. Ti-substitution mechanism in plutonic oxykaersutite from the Larvik alkaline complex, Oslo rift, Norway. Mineralogical Magazine 68, 687–697.
Siebert, L., Simkin, T., Kimberly, P., 2010. Volcanoes of the World. University of California Press, pp. 2010–2551.
Silva, L.C., Mendes, M.H., Torres, P.C., Palácios, T., Munhá, J., 1997. Petrografia das Formações Vulcânicas da Erupção de 1995 na Ilha do Fogo, Cabo Verde. In: Réffega, A., et al. (Eds.), A Erupção Vulcânica de 1995, na Ilha do Fogo, Cabo Verde. IICT, Lisboa, pp. 164–170.
Staudigel, H., Park, K.H., Pringle, M., Rubenstone, J.L., Smith, W.H.F., Zindler, A., 1991. The longevity of the South-Pacific isotopic and thermal anomaly. Earth and Planetary Science Letters 102, 24–44.
Stracke, A., Bourdon, B., 2009. The importance of melt extraction for tracing mantle heterogeneity. Geochimica et Cosmochimica Acta 73, 218–238.
Stracke, A., Hofmann, A.W., Hart, S.R., 2005. FOZO, HIMU, and the rest of the mantle zoo. Geochemistry, Geophysics, Geosystems 6, Q05007. http://dx.doi.org/10.1029/2004GC000824.
Stroncik, N.A., Klügel, A., Hansteen, T.H., 2009. The magmatic plumbing system beneath El Hierro (Canary Islands): constraints from phenocrysts and naturally quenched basaltic glasses in submarine rocks. Contributions to Mineralogy and Petrology 157, 593–607.
Torres, P.C., Madeira, J., Silva, L.C., Brum da Silveira, A., Serralheiro, A., Mota Gomes, A., 1998. Carta Geológica das Erupções Históricas da Ilha do Fogo (Cabo Verde): revisão e actualização. Comunicações do Instituto Geológico e Mineiro 84, A193–196.
Torres, P., Silva, L.C., Munhá, J., Caldeira, R., Mata, J., Tassinari, C., 2010. Petrology and geochemistry of lavas from Sal Island: implications for the variability of the Cape Verde magmatism. Comunicações Geológicas 97, 35–62.
Trindade, M.J., Mata, J., Munhá, J., 2003. Petrogenesis of the quaternary magmatism from the S. Vicente Island (Cape Verde). Comunicações do Instituto Geológico e Mineiro 90, 169–188.
Vervoort, J., Patchett, P., Blichert-Toft, J., Albarède, F., 1999. Relationships between Lu-Hf and Sm-Nd isotopic systems in the global sedimentary system. Earth and Planetary Science Letters 168, 79–99.
Vinnik, L., Silveira, G., Kiselev, S., Farra, V., Weber, M., Stutzmann, E., 2012. Cape Verde hotspot from the upper crust to the top of the lower mantle. Earth and Planetary Science Letters 319-320, 259–268.
Wang, K., Plank, T., Walker, J.D., Smith, E.I., 2002. A mantle melting profile across the basin and range, SW USA. Journal of Geophysical Research 107 (ECV 5, 1-21).
Watson, S., McKenzie, D., 1991. Melt generation by plumes: a study of Hawaiian volcanism. Journal of Petrology 32, 501–537.
Weis, D., Kieffer, B., Maerschalk, C., Barling, J., de Jong, J., Williams, G., Hanano, D., Pretorius, W., Mattielli, N., Scoates, J., Goolaerts, A., Friedman, R., Mahoney, J., 2006. High-precision isotopic characterization of USGS reference materials by TIMS and MC-ICP-MS. Geochemistry, Geophysics, Geosystems 7. http://dx.doi.org/10.1029/2006GC001283.
White, W.M., 2015. Isotopes, DUPAL, LLSVPs, and Anekantavada. Chemical Geology 419, 10–28.
Williams, C., Hill, I., Young, R., White, R.S., 1990. Fracture zones across the Cape Verde rise, NE Atlantic. Journal of the Geological Society of London 147, 851–857.
Wilson, D., Peirce, C., Watts, A., Grevemeyer, I., Krabbenhoeft, A., 2010. Uplift at lithospheric swells-I: seismic and gravity constraints on the crust and uppermost mantle structure of the Cape Verde mid-plate swell. Geophysical Journal International 182, 531–550.
Wilson, D., Peirce, C., Watts, A., Grevemeyer, I., 2013. Uplift at lithospheric swells-II: is the Cape Verde mid-plate swell supported by a lithosphere of varying mechanical strength? Geophysical Journal International 193, 798–819.
Ziberna, L., Klemme, S., Nimis, P., 2013. Garnet and spinel in fertile and depleted mantle: insights from thermodynamic modelling. Contributions to Mineralogy and Petrology 166, 411–421.
Zindler, A., Hart, S.R., 1986. Chemical geodynamics. Annual Review of Earth and Planetary Sciences 14, 493–571.